# Braking Capabilities on Flooded Runways

Julio Atarés, Sara Lagunas (Airbus),
Gerard van Es, Peter van der Geest (NLR)

Short abstract: Future Sky Safety is a Joint Research Programme (JRP) on Safety, initiated by EREA, the association of European Research Establishments in Aeronautics. The Programme contains two streams of activities: 1) coordination of the safety research programmes of the EREA institutes and 2) collaborative research projects on European safety priorities.

This deliverable is produced by the Project *Solutions for Runway Excursions*. The main objective of this study is to obtain and analyse flight test data on braking performance on water contaminated runways.



| | |
|---|---|
| **Programme Manager** | M.A. Piers, NLR |
| **Operations Manager** | L.J.P. Speijker, NLR |
| **Project Manager (P3)** | G.W.H. van Es, NLR |
| **Grant Agreement No.** | 640597 |
| **Document Identification** | D3.8 |
| **Status** | Approved |
| **Version** | 2.0 |
| **Classification** | Public |

*This page is intentionally left blank*




Future Sky Safety has received funding from the EU's Horizon 2020 Research and Innovation Programme, under Grant Agreement No. 640597.

## Contributing partners

| Company | Name |
|---|---|
| **Airbus Defence** | Julio Atarés |
| **Airbus Defence** | Sara Lagunas |
| **NLR** | Gerard van Es |
| **NLR** | Peter van der Geest |

## Document Change Log

| Version | Issue Date | Remarks |
|---|---|---|
| 1.0 | 08-03-2019 | First formal release |
| 2.0 | 08-04-2019 | Second formal release |

## Approval status

| **Prepared by:** *(name)* | **Company** | **Role** | **Date** |
|---|---|---|---|
| J. Atarés | NLR | Main Author | 05-10-2018 |
| **Checked by:** *(name)* | **Company** | **Role** | **Date** |
| A. Rutten | NLR | Quality Assurance | 01-04-2019 |
| **Approved by:** *(name)* | **Company** | **Role** | **Date** |
| G.W.H van Es | NLR | Project Manager (P3) | 08-03-2019 |
| L.J.P. Speijker | NLR | Operations Manager | 08-04-2019 |




Future Sky Safety has received funding from the EU's Horizon 2020 Research and Innovation Programme, under Grant Agreement No. 640597.

## Acronyms

| Acronym | Definition |
|---|---|
| A/C | Aircraft |
| ASDA | Accelerate-Stop Distance Available |
| $C_{Dh}$ | Hydrodynamic Drag Coefficient |
| $C_{Lh}$ | Hydrodynamic Lift Coefficient |
| DGPS | Differential Ground Positioning System |
| $\frac{d\omega}{dt}$ | Wheel Rotational Acceleration |
| $D_h$ | Hydrodynamic Drag |
| $D_{i\ av}$ | Average Depth at sub-pond i |
| $D_{i\ 3.1\ m}$ | Depth along the line located 3.1 m away from runway centreline, at |
| DOF | Direction of Flight |
| DOT | Direction of Taxi |
| EASA | European Aviation Safety Agency |
| EC | European Committee |
| ESDU | Engineering Sciences Data Unit |
| FAA | Federal Aviation Administration |
| $F_{brk}$ | Braking Force |
| $F_{disp+imp}$ | Displacement and Impingement Drag |
| $F_{roll}$ | Rolling Friction Force |
| FSS | Future Sky Safety |
| FTR | Flight Test Request |
| GS | Ground Speed |
| I | Wheel Moment of Inertia |
| K | Aquaplaning Speed Factor |
| $L_{conta}$ | Contaminant Lift |
| LDA | Landing Distance Available |
| LG | Landing Gear |
| $L_h$ | Hydrodynamic Lift |
| $M_{Brake}$ | Braking Torque |
| MLG | Main Landing Gear |




Future Sky Safety has received funding from the EU's Horizon 2020 Research and Innovation Programme, under Grant Agreement No. 640597.

| Acronym | Definition |
|---|---|
| NASA | National Aeronautics and Space Administration |
| NLG | Nose Landing Gear |
| N | Normal Reaction |
| NLR | National Aerospace Laboratory |
| $p_{\text{bearing tire}}$ | Tire Bearing Pressure |
| $p_{\text{tire}}$ | Tire Inflation Pressure |
| r | Tire Radius |
| R | Wheel Radius |
| $r_d$ | Deflected Tire Radius |
| RWY | Runway |
| $\text{slope}_i$ | Runway longitudinal slope at sub-pond i |
| $S_{refD}$ | Reference Surface for Hydrodynamic Drag |
| $S_{refL}$ | Reference Surface for Hydrodynamic Lift |
| TODA | Take-off Distance Available |
| TORA | Take-off Run Available |
| V | Speed |
| $V_p$ | Aquaplaning Speed |
| WP | Work Package |
| $X_{Braking}$ | Braking Friction Force on the tire, on runway axes |
| $X_{contaminant}$ | Contaminant Drag on the tire, on runway axes |
| $X_{rolling}$ | Rolling Friction Force on the tire, on runway axes |
| $x_c$ | Horizontal position of the contact point between tire and runway, with |
| Z | Normal load on the tire, on runway axes |
| $\mu_{Brake}$ | Braking Friction Coefficient |
| $\mu_{effective}$ | Effective Braking Friction Coefficient |
| $\mu_{Roll}$ | Rolling Friction Coefficient |
| $\eta_{A/S}$ | Antiskid Efficiency |
| $\omega$ | Wheel Rotational Speed |
| $\rho_w$ | Water Density |




Future Sky Safety has received funding from the EU's Horizon 2020 Research and Innovation Programme, under Grant Agreement No. 640597.

# EXECUTIVE SUMMARY


## Problem Area

The fast majority of aircraft takeoffs and landings is conducted on dry runways. Only a small portion is conducted on non-dry runways like water contaminated (flooded) runways. Statistics show that the likelihood of a runway excursion during takeoff or landing is much higher on flooded runways than on dry runways. Extreme loss of tyre braking can occur during rejected takeoffs and Landings on flooded runways. As a result the stopping distance increases significantly and could exceed the available runway length. Most research in the past has focused on the braking capabilities of aircraft on wet runways instead of water contaminated runways. Most of the knowledge of aircraft braking performance on water contaminated runways was gained during the late 60s and mid-70s. This knowledge is still used to determine the takeoff and landing performance of today's modern aircraft. During the development of the European Action Plan for the Prevention of Runway Excursions it was recognised that current aircraft designs may act differently when braking on water contaminated runways, from aircraft tested in the 60s and 70s, due to new tyres and antiskid system designs.

## Description of Work

Flight tests using a Cessna Citation aircraft on a flooded runway are conducted as part of the Project Solutions for runway excursions (P3) within the FUTURE SKY SAFETY programme. The objective of this task is to obtain and analyse flight test data on braking performance on water contaminated runways. Effective braking friction for different grounds speeds are derived, contamination drag levels are established, and insight into the hydroplaning characteristics under un-braked and braked conditions is obtained.

## Results & Conclusions

This report summarises the flight tests conducted with a Cessna Citation II and an Airbus A400M aircraft on a flooded runway. Un-braked and braked tests were conducted in a specially constructed water pond at different ground speeds. Numerous parameters were recorded during each test run including accelerations, speeds, engine performance, etc. From the test data, effective braking friction for different grounds speeds were derived, contamination drag levels were established, and insight into the hydroplaning characteristics under un-braked and braked conditions were obtained. This leads to better understanding of aircraft ground handling performance flooded runway conditions.

Major flight test findings from the analysis of data obtained for the business jet (Cessna Citation II) are:

- Ground speed was identified as major a factor that influences flooded-runway tyre friction performance;
- The tyre friction performance for flooded runway conditions is significantly less than for a wet runway;
- Braking capabilities for a water depth of 9.9 mm is comparable to that for 16.7 mm depth.





Future Sky Safety has received funding from the EU's Horizon 2020 Research and Innovation Programme, under Grant Agreement No. 640597.

- Hydroplaning has a large influence on the anti-skid performance of the Cessna Citation test aircraft. It is shown that locked wheel conditions can occur despite the locked wheel crossover protection system.

Regarding findings obtained from analysis of the Airbus A400M tests, 4 main points are to be highlighted:

- In terms of **displacement drag**, a 3$^{rd}$ order regression was built, as a function of both ground speed and average depth seen by the wheel. This shows adequate consistency with the model proposed by ESDU 90035 (Ref. [2]).
- In terms of **aquaplaning speed**, if the most conservative results are considered, aquaplaning is estimated to take place between 80 and 90 kt. This is consistent with the results obtained by NLR in their Cessna Citation tests (which estimated aquaplaning to occur between 84 and 92 kt.
- In terms of **rolling friction**, its measurements during the test campaign were consistent with the expected results. In consequence, they were used for the estimation of effective braking friction coefficient.
- In terms of **braking friction**, results at tire level indicated, as in the case of aquaplaning speed, consistency with previous tests performed on the same runway.

## Applicability

The results of the tests can be used to review and improve current EASA means of compliance related to contaminated runway performance. This work is planned in follow-up activities of Future Sky Safety P3.




Future Sky Safety has received funding from the EU's Horizon 2020 Research and Innovation Programme, under Grant Agreement No. 640597.

*This page is intentionally left blank*




Future Sky Safety has received funding from the EU's Horizon 2020 Research and Innovation Programme, under Grant Agreement No. 640597.

# TABLE OF CONTENTS

# LIST OF FIGURES






Future Sky Safety has received funding from the EU's Horizon 2020 Research and Innovation Programme, under Grant Agreement No. 640597.

Future Sky Safety has received funding from the EU's Horizon 2020 Research and Innovation Programme, under Grant Agreement No. 640597.

# LIST OF TABLES






Future Sky Safety has received funding from the EU's Horizon 2020 Research and Innovation Programme, under Grant Agreement No. 640597.

# 1 INTRODUCTION

## 1.1. The Programme

FUTURE SKY SAFETY is an EU-funded transport research programme in the field of European aviation safety, with an estimated initial budget of about € 30 million, which brings together 32 European partners to develop new tools and new approaches to aeronautics safety, initially over a four-year period starting in January 2015.

In this first phase of the Programme, one of the research focuses on four main topics:

- Building ultra-resilient vehicles and improving the cabin safety
- Reducing risk of accidents
- Improving processes and technologies to achieve near-total control over the safety risks
- Improving safety performance under unexpected circumstances

The Programme will also help coordinate the research and innovation agendas of several countries and institutions, as well as create synergies with other EU initiatives in the field (e.g. SESAR, Clean Sky 2).

FUTURE SKY SAFETY contributes to the EC Work Programme Topic MG.1.4-2014 Coordinated research and innovation actions targeting the highest levels of safety for European aviation, in Call/Area Mobility for Growth – Aviation of Horizon 2020 Societal Challenge Smart, Green and Integrated Transport. FUTURE SKY SAFETY addresses the Safety challenges of the ACARE Strategic Research and Innovation Agenda (SRIA).

## 1.2. Project context

Within the FUTURE SKY SAFETY programme the project Solutions for runway excursions (P3) was initiated to tackle the problem of runway excursions. A runway excursion is the event in which an aircraft veers off or overruns the runway surface during either take-off or landing. Safety statistics show that runway excursions are the most common type of accident reported annually, in the European region and worldwide. There are at least two runway excursions each week worldwide. Runway excursions are a persistent problem and their numbers have not decreased in more than 20 years.

Runway excursions can result in loss of life and/or damage to aircraft, buildings or other items struck by the aircraft. Excursions are estimated to cost the global industry about $900M every year. There have also been a number of fatal runway excursion accidents. These facts bring attention to the need to identify measures to prevent runway excursions.

Several studies were conducted on this topic. Most recently a EUROCONTROL sponsored research “Study of Runway Excursions from a European Perspective” showed that the causal and contributory factors leading to a runway excursion were the same in Europe as in other parts of the world. The study findings made extensive use of lessons from more than a thousand accident and incident reports. Those lessons were used to craft the recommendations contained in the European Action Plan for the Prevention of Runway Excursions, which was published in January 2013. This action plan is a deliverable of the European

Aviation Safety Plan, Edition 2011-2014. The European Action Plan for the Prevention of Runway Excursions provides practical recommendations and guidance materials to reduce the number of runway excursions in Europe.

The Action Plan also identified areas where research is needed to further reduce runway excursion risk.

The present project focuses on a number of these identified areas. Four areas of research were selected for which additional research is needed:

1. Research on the flight mechanics of runway ground operations on slippery runways under crosswind conditions.
2. Research on the impact of fluid contaminants of varying depth on aircraft stopping performance.
3. Research on advanced methods for analysis of flight data for runway excursion risk factors.
4. Research into new technologies to prevent excursions or the consequences of excursions.

This study addresses the impact of fluid contaminants of varying depth on aircraft stopping performance.

## 1.3. Research objectives

The objective of this task is to obtain and analyse flight test data on braking performance on water contaminated runways. More specifically, the obtained flight test data are used:

- To derive effective braking friction for different grounds speeds;
- To establish contamination drag levels, and
- To obtain insight into the hydroplaning characteristics under un-braked and braked conditions.

This leads to better understanding of aircraft ground handling performance flooded runway conditions.

## 1.4. Structure of the document

Section 2 includes a brief theoretical background on forces acting on a single tire in contaminated operations. Section 3 and 4 details the test requirements, strategy, facilities, and test results for the business jet and large transport aircraft. Finally, section 5 provides the conclusions.




Future Sky Safety has received funding from the EU's Horizon 2020 Research and Innovation Programme, under Grant Agreement No. 640597.

# 2 THEORETICAL BACKGROUND

Aircraft performance on water contaminated surfaces is influenced by three sources of retarding force:

1. **Contaminant drag**, caused by fluid displacement by the landing gear (**Displacement Drag**) and fluid impingement on airframe and wing surfaces, as well as between landing gear legs (**Impingement Drag**). Both components can be accurately represented as a single horizontal retarding force (Figure 1).

   Additionally, contaminant produces a hydrodynamic lift ($L_{conta}$), also represented.

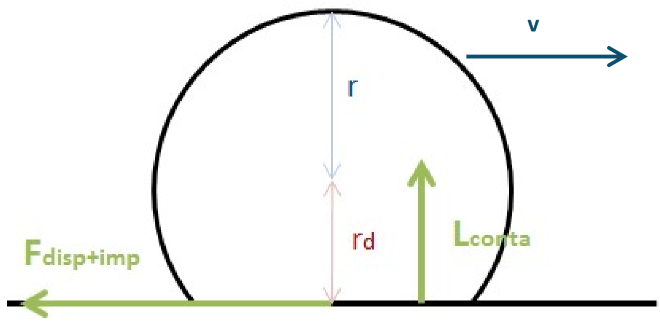


**Figure 1 Contaminant forces (displacement and impingement drag, and hydrodynamic lift), acting on a single tire**

In Figure 1, *r* represents the nominal tire radius; rd represents the deflected tire radius, and $F_{disp+imp}$ represents the global contribution of displacement and impingement drag.

2. **Rolling friction** ($F_{roll}$), due to tire deformation as it rolls along the runway surface. In fact, rolling deformation displaces normal reaction (*N*) application point to a certain forward distance from the wheel axle (Figure 2).

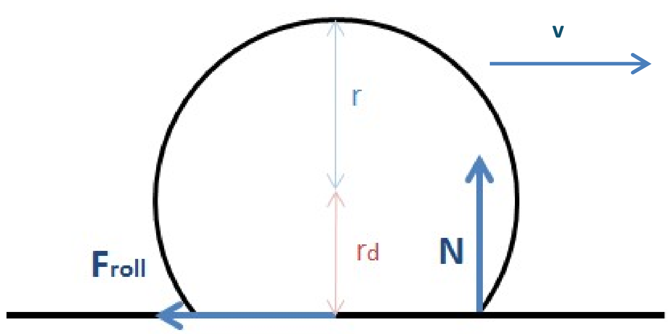


**Figure 2 Rolling friction drag and displacement of normal force application, due to tire deformation**

3. **Braking friction** (Fbrk), which counteracts the torque generated by the brakes when these are activated. (Figure 3).

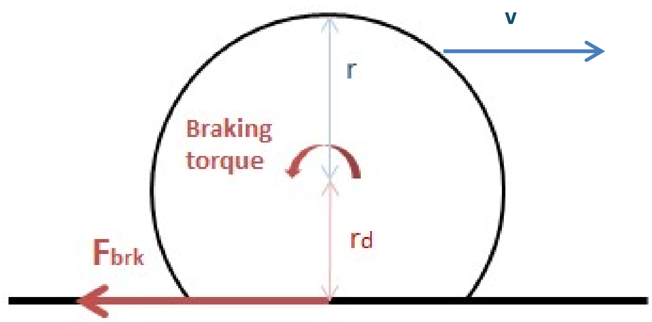


**Figure 3 Braking force acting on a tire.**

Figures 4 and 5 show all the forces a wheel is subjected to in an un-braked and a braked operation. As can be seen, in both cases, several horizontal retarding components appear: rolling friction and contaminant drag in the un-braked case, and braking friction, rolling friction and contaminant drag in the braked one.

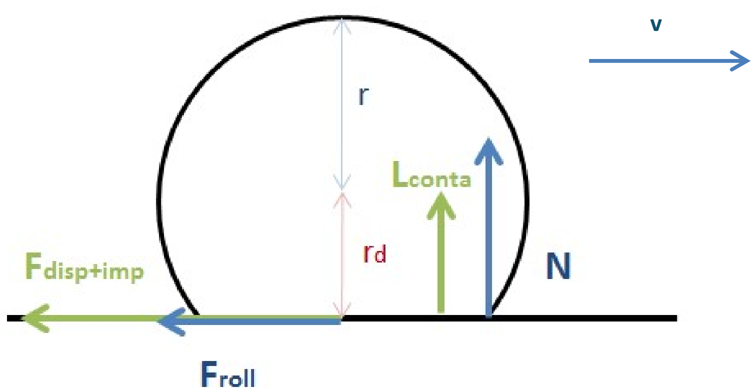


**Figure 4 Forces acting on an un-braked tire, when operating under contaminated conditions**

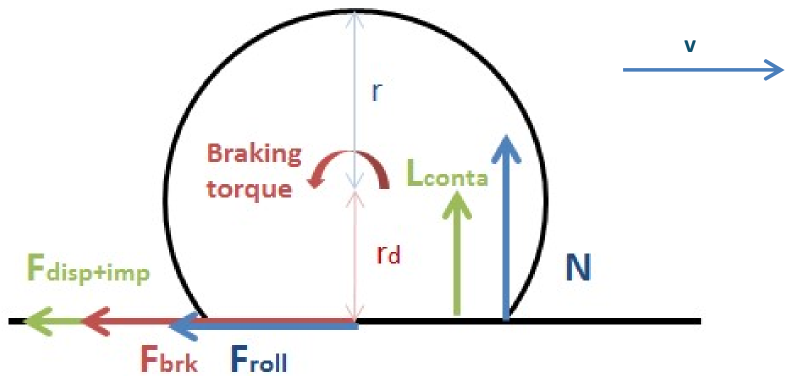


**Figure 5 Forces acting on a braked tire, when operating under contaminated conditions**




Future Sky Safety has received funding from the EU's Horizon 2020 Research and Innovation Programme, under Grant Agreement No. 640597.

# 3 FLIGHT TEST RESULTS OBTAINED WITH A BUSINESS JET

## 3.1. Flight test programme

### 3.1.1 Flight test aircraft

NLRs research aircraft, a Cessna Citation II, was used for the flight test programme described in this report (see Figure 6Figure 6). Originally designed for executive travel, the NLR Cessna Citation II test aircraft (registration PH-LAB) has been extensively modified by NLR to serve as a versatile research and test platform. Table 1 provides some basic data on the performance of the Cessna Citation II. The aircraft has two Pratt & Whitney JT15D-4 turbofan engines each rated 2,500 pounds of thrust. The aircraft is equipped with a fully modulating anti-skid braking system (MKIII). The system detects incipient skids by using a wheel speed transducer to measure the deceleration of each landing wheel, and then prevents skids by reducing the brake pressure in proportion to the deviation of each wheel from normal braking deceleration. The system modulates brake pressure to maximize braking efficiency. The left and right wheel brakes are hydraulically operated by independent master cylinders attached to the pilot's and copilot's rudder pedals. The brake system is pressurised when either pilot depresses the toe pedals. Interconnect assemblies allow either pilot to operate the brakes with equal authority. The single-wheel main gear used 22 × 8, 24 P.R., type VII aircraft tyres. The tyre inflation pressures were 115 psi for the main-gear tyres and maintained within ±5 psi throughout the course of the test programme. The main gear tyres as well as the brake units were not new. The left hand tyre had a tread depth of 5.2 mm at the start of the test programme and the right hand main gear tyre had a tread depth of 4.8 mm. When the tests were finished this had reduced to 5.1 and 4.6 mm respectively. The aircraft was configured for the Future Sky Safety Contaminated Runway campaign to enable measurement of lateral and longitudinal acceleration, wheel speed rotation by using the aircrafts anti-skid system and pressure in the low pressure pilot brake system. The aircraft was operated by NLR flight crews.




Future Sky Safety has received funding from the EU's Horizon 2020 Research and Innovation Programme, under Grant Agreement No. 640597.

**Table 1 Some data on the Citation II aircraft.**

| | |
|---|---|
| Altitude | |
| Maximum operating altitude | Approx. 43,000 ft |
| Speed | |
| Maximum speed (sea level to 9,300 m / 30,500 ft) | 262 KIAS, Mach 0.705 |
| Weight | |
| Maximum Take-off Weight [extended] | 6,400 kg (14100 lbs) [14600 lbs] |
| Maximum Landing Weight | 6,100 kg (13500 lbs) |
| Dimensions | Length 14.40 m |
| | Wingspan 15.91 m |
| | Height 4.58 m |
| | Main gear width 5.36m (centre of wheels) |
| Performance | |
| Take-off distance (MTOW) Landing distance (MLW) | 1,050 m (3450 ft) 745 m (2450 ft) |


**Figure 6 NLR Cessna Citation test aircraft.**

### 3.1.2 Test site

The flight testing was executed in the Netherlands at the airport of Twente (EHTW). This airport has a long and wide runway ideally for flight testing (see Figure 7). The runway has a Possehl Antiskid top layer with an average macrotexture depth of 1.4 mm. The airport was closed for all other aircraft during the flight tests.

### 3.1.3 Weather conditions

Weather conditions were recorded by an official weather station next to the runway. Also some weather data like temperature and static pressure were recorded on-board of the aircraft. The tests were conducted in 2016 and 2018 over two consecutive days. In 2016, during the first day of testing the air temperature varied between 27 and 29 deg. C. Wind speeds varied between 7-10 kt. with a mean direction of 67 deg. There were no clouds during the first day of testing. During the second day the weather had changed. The air temperature now varied between 19 and 21 deg. C. The wind speed varied between 8-11 kt. with a mean direction of 190 deg. During the second day the sky was mainly clouded. However, no precipitation was recorded. In 2018, during the first day of testing the air temperature varied between 20 and 26 deg. C. Wind speeds varied between 4-8 kt. with a mean direction of 90 deg. There were no clouds during the first day of testing. During the second day of testing the air temperature varied between 20 and 25 deg. C. Wind speeds varied between 2-4 kt. with a variable directions. No precipitation was recorded during both days of testing.




Future Sky Safety has received funding from the EU's Horizon 2020 Research and Innovation Programme, under Grant Agreement No. 640597.

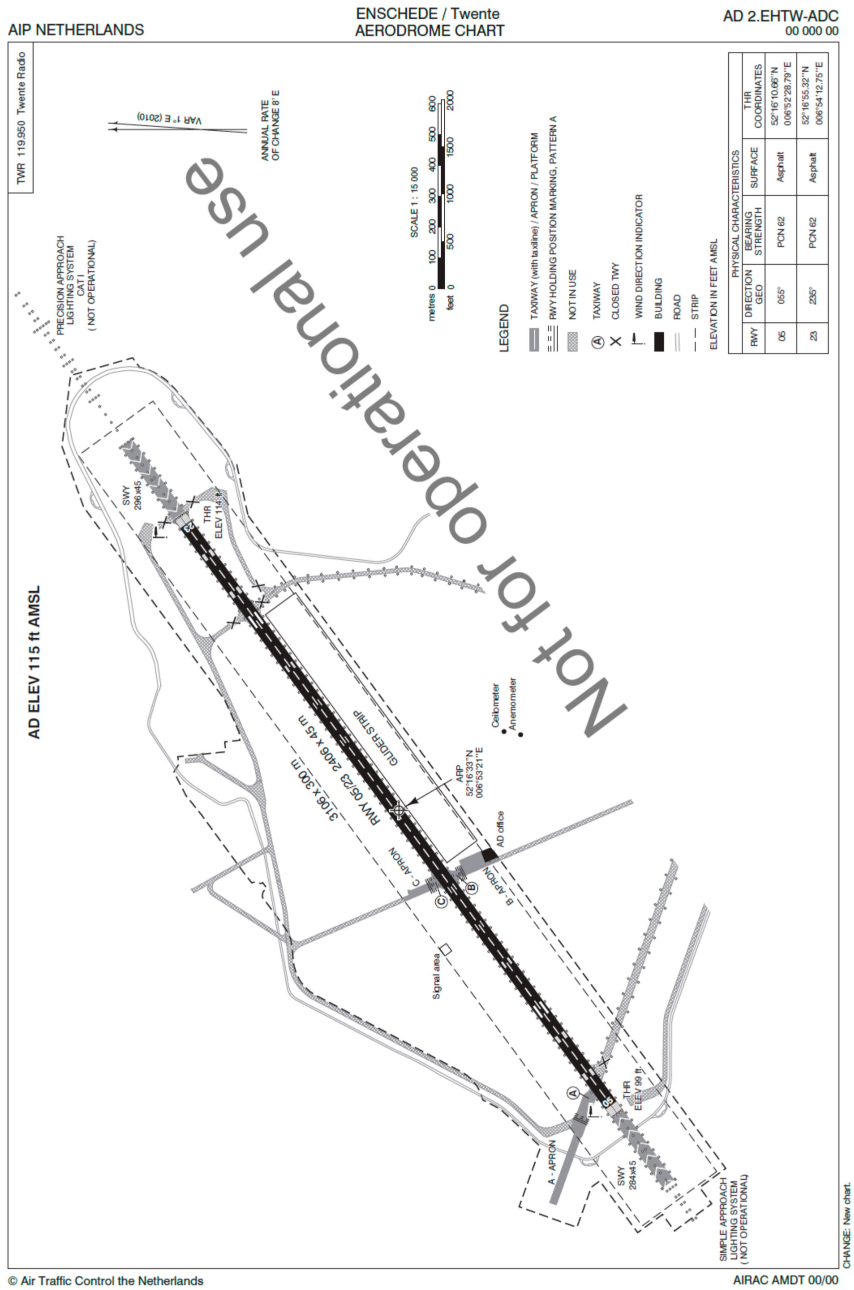


**Figure 7 Aerodrome chart Twente airport.**

## 3.1.4 Water pond construction

The initial objective of the test programme requires a runway covered with a target depth of 15 mm of standing water. A lower water depth of 8-10 mm was pursued during the second test programme conducted in 2018. The build-in cross slope of the runway prevents that such a quantity of water stays on the runway, unless there is heavy rainfall. A water pond is therefore needed to create an area of sufficient water depth that stays at this level for long enough time for an aircraft to pass. Such water ponds are normally build using flexible re-enforced rubber strips as dikes to contain the water. These rubber strips are then put into grooves that are made into the runway surface (see Figure 8). This is a classical way of building a water pond on a runway. It has been used for water certification ingestion tests as well as for braked tests with a wide range of civil transport aircraft since the 1960s. For instance both the Citation and the A400M have been tested in such water ponds for certification purposes. NLR has also tested the Citation in a water pond for another project in 1997 (unbraked test only).

**Figure 8 Flexible rubber strip in a runway groove.**

The runway at Twente did not have a water pond facility at the start of the project. This facility had to be constructed. A classical water pond consists of series of grooves into which flexible rubber strips are put to form dikes. To gain some experience with such a setup, a small test pond was constructed at the NLR premises before making one at Twente airport. This water pond measured 4 by 10 m and is shown in




Future Sky Safety has received funding from the EU's Horizon 2020 Research and Innovation Programme, under Grant Agreement No. 640597.

Figure 9 (empty). The test pond was filled to several water levels. Experiences were gained in grooving, fixing the rubber strips into the grooves, measuring of water depths and managing leakage of the pond.

**Figure 9 Test water pond.**

After positive experiences gained with the test water pond it was decided to construct the pond at the test location. The runway at Twente has a very consistent longitudinal slope of 0.2% along the runway. Likewise the cross slope is also very consistent along the runway being 0.6-0.8% near the runway centreline (within 5 m) and 1.5-1.6% further away from the centreline. The longitudinal slope required that several rubber cross dams had to be constructed to get reasonable consistent water levels in the water pond. These cross dams were placed every 7.7 m to form 13 separate sections. The final water pond is shown in Figure 10. As the aim of the flight tests is to analyse braking performance it is not necessary to have the nosewheel running through the water. Therefore no pond was construction for the nosewheel to run through. Keeping the centre part dry also provides additional controllability in case the aircraft deviates from its track during the test run.




Future Sky Safety has received funding from the EU's Horizon 2020 Research and Innovation Programme, under Grant Agreement No. 640597.

**Figure 10 Water pond at Twente airport.**

The overall length of the water pond was 100 m. This is sufficient long to obtain useful test data. Braked tests done by NASA using a B727 and B737 used a similar length. The water pond starts 1.15 m from the centreline and stretches to 5 m from the centreline. The target average water depth at the main wheels was set to 15 mm. Along each section the actual water depth will normally vary both in longitudinal as well as in lateral direction as the test section is not completely flat. However the main gear tyres should be exposed to target water depth when the aircraft does not deviate significantly from the runway centreline. Deviations from the centreline were recorded on a few test runs, however, these were not significant enough (0.5 m or less) to influence the test results.


**Figure 11 Filling of the water pond.**


**Figure 12 Water depth gauge.**




Future Sky Safety has received funding from the EU's Horizon 2020 Research and Innovation Programme, under Grant Agreement No. 640597.

The water pond was filled to the required depth using water trucks as shown in Figure 11. Water depths were measured using a specially constructed wedge which is shown in Figure 12. Prior to each run water depth measurements were taken and recorded at pre-defined positions in each section of the water pond (see Figure 13). These positions matched the location of the main gear tyres. If the water depth was well off the target value, water was either removed from the section or added. High winds can make it difficult to maintain consistent water levels. Based on previous experiences with water pond testing a maximum wind speed of 12 kt. was defined for the test programme. Figure 14 and Figure 15 show the surface of the water pond under calm and light windy conditions. In order to minimise the influence of wind on the water depth measurements, a metal ring was placed around the water depth gauge as illustrated in Figure 16.

**Figure 13 Example of measuring water depth level in each section.**

**Figure 14 Water pond in calm wind conditions**

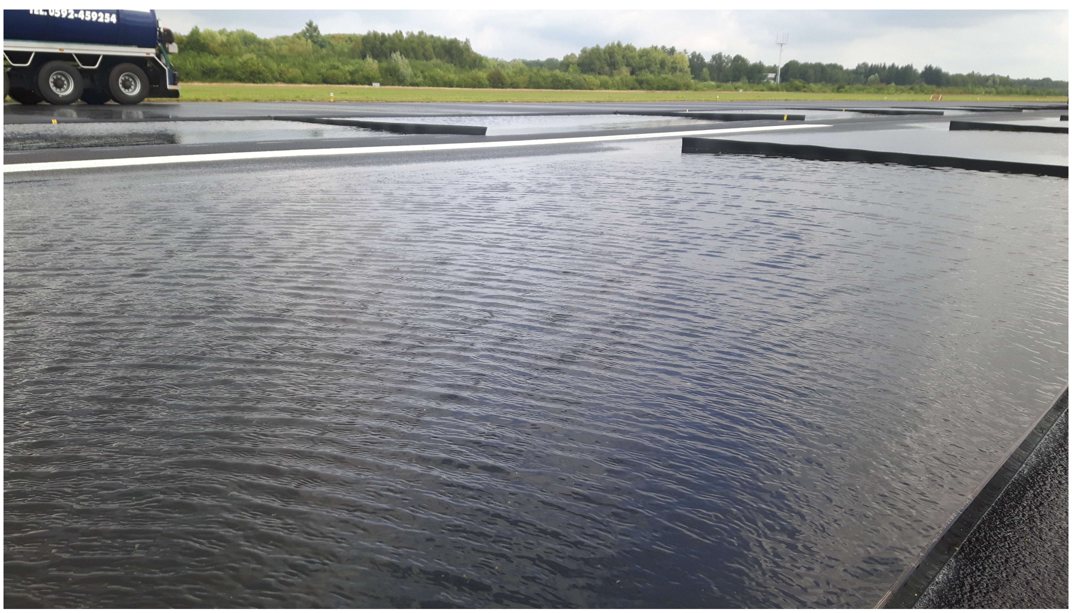


**Figure 15 Water pond at 8 kt. wind.**

**Figure 16 Measuring of water depth using a metal ring around the water depth gauge.**

The target water depth was set to 15 mm at the main gear tyre track during the first flight tests in 2016. During the 2016 test programme the overall average water depth level was somewhat higher than this target (16.7 mm). This was not considered a major issue for the objectives of the project. The average water depths for each test run varied between 14 and 19.2 mm. An example of the measured water depths in the different test sections is shown in Figure 17. Two measurements were taken in each left and right section. The direction of flight is from section 1 to 13. During the second flight test programme (2018 tests) a lower water depth was used with a target of 8-10 mm. During the 2018 test programme the overall average water depth level was 9.9 mm with only minor variations between each run (9.6-10.1 mm).




Future Sky Safety has received funding from the EU's Horizon 2020 Research and Innovation Programme, under Grant Agreement No. 640597.

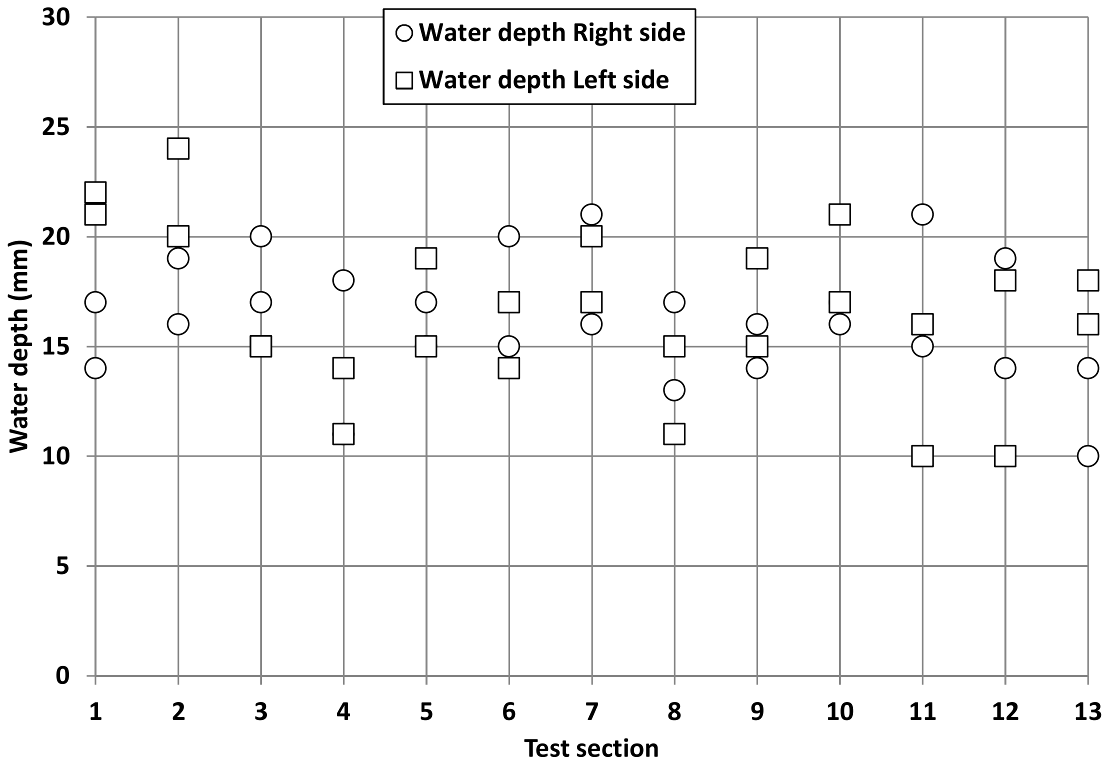


**Figure 17 Example of the water depth levels measured along the water pond (numbers refer to section).**

### 3.1.5 Text matrix

The test matrix was developed keeping in mind how the data reduction process would be done. As an aircraft passes through the water pond, the tyres displace the water. This causes a drag force acting on the tyres called displacement drag. Water thrown up by the tyres could hit the airframe causing an impingement drag force (see Figure 18). To account for these drag forces tests runs in an unbraked condition were required. Therefore the test matrix had to incorporate both an unbraked and a braked run for a given target entry speed. It is important that true airspeed and ground speed during the water pond passage are more or less equal for both test pairs. The aircraft weight should be similar or equal in both test-pairs, as well as the average water depth and control surfaces deflections. The aircraft was tested with flaps in the up position during all runs. The runs were arranged in such a way that there was a build-up approach as to the water pond entry speeds. This was done from a flight safety point of view. The maximum test speeds were determined by the rotation speed of the aircraft which depends on flaps setting and aircraft weight. Table 2 shows the test matrix. For the 2018 tests one additional point was added (50 kts target entry speed).

Initially is was felt that at the higher speeds test runs with half the braking input would be needed to make the test pilots aware of the aircraft behaviour. However, during the actually testing it was decided that these partial-braked runs were not needed (test points 6, 9 and 12).

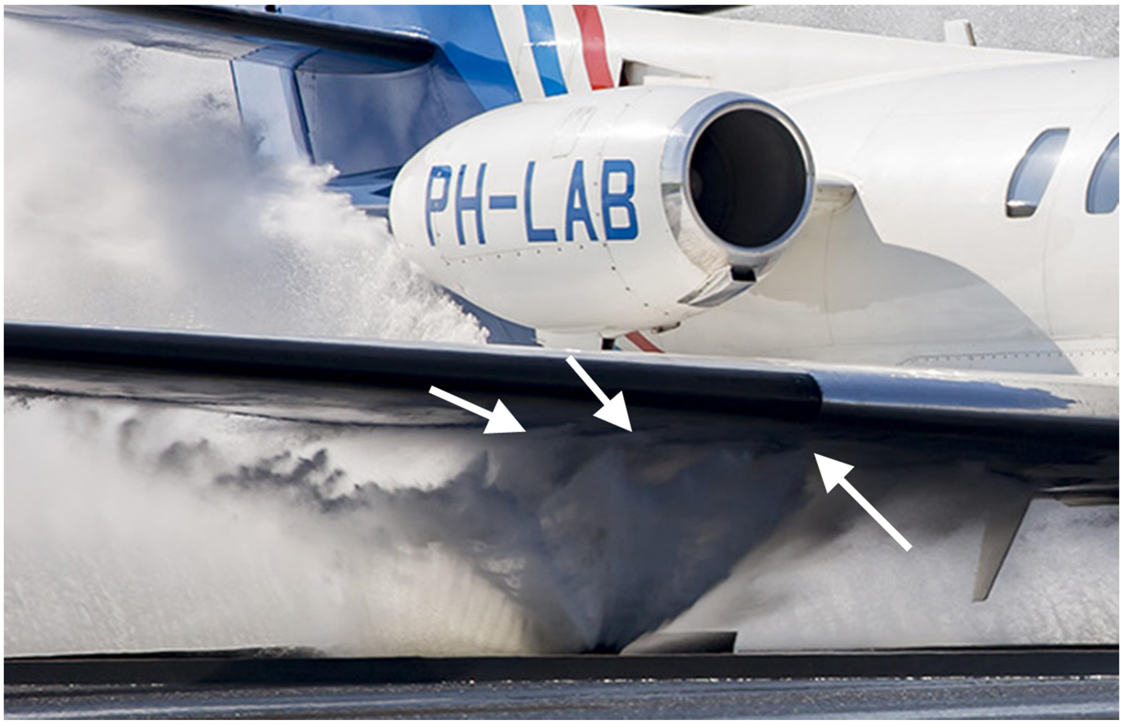


**Figure 18 Water spray hitting the airframe.**

### Table 2 Test matrix

| Test number | Flight Configuration (Pitch, Weight and Flaps,) | Engine setting | Target water pond entry speed IAS (kt.) | Description |
|---|---|---|---|---|
| 1 | Takeoff, takeoff weight, flaps configuration up | Idle | 60 | Unbraked |
| 2 | Takeoff, takeoff weight, flaps configuration up | Idle | 60 | Maximum braking |
| 3 | Takeoff, takeoff weight, flaps configuration up | Idle | 70 | Unbraked |
| 4 | Takeoff, takeoff weight, flaps configuration up | Idle | 70 | Maximum braking |
| 5 | Takeoff, takeoff weight, flaps configuration up | Idle | 80 | Unbraked |
| 6 | Takeoff, takeoff weight, flaps configuration up | Idle | 80 | half pressure/moderate braked |
| 7 | Takeoff, takeoff weight, flaps configuration up | Idle | 80 | Maximum braking |
| 8 | Takeoff, takeoff weight, flaps configuration up | Idle | 90 | Unbraked |
| 9 | Takeoff, takeoff weight, flaps configuration up | Idle | 90 | half pressure/moderate braked |
| 10 | Takeoff, takeoff weight, flaps configuration up | Idle | 90 | Maximum braking |
| 11 | Takeoff, takeoff weight, flaps configuration up | Idle | 100 | Unbraked |
| 12 | Takeoff, takeoff weight, flaps configuration up | Idle | 100 | half pressure/moderate braked |
| 13 | Takeoff, takeoff weight, flaps configuration up | Idle | 100 | Maximum braking |




Future Sky Safety has received funding from the EU's Horizon 2020 Research and Innovation Programme, under Grant Agreement No. 640597.

### 3.1.6 Test run execution

For the water pond tests a detailed flight test plan was written that included a safety assessment. This flight test plan was reviewed by external experts (test pilots). The detailed flight test plan is presented in [Tump & Van Es, (2016)].

For each test run the water pond was filled to the target water depth level. The aircraft was positioned at a pre-determined distance from the water pond. As soon as the water pond was ready, the aircraft would start its engines. A static takeoff was then commenced. The engines were set to idle at a marked position before the water pond. The position of the idle thrust marker and the position for the static takeoff were determined as such as the aircraft would enter the water pond near the target speed and with the engines in idle thrust. The calculations for this were done using an accurate in-house developed performance program. An example of a typical run is shown in Figure 19. This shows the time-history plot of the (uncorrected) longitudinal acceleration and the ground speed. As can be seen from the plot the aircraft is accelerated to a certain speed from the static takeoff. After reaching the idle marker the engines were set to idle at which the normal acceleration starts to drop. As the aircraft reaches the water pond the aircraft is slightly decelerating due to aerodynamic and rolling friction forces being larger than the idle forward thrust. This was the case for all test runs conducted. When entering the water pond the aircraft starts to decelerate more as illustrated in Figure 19. Depending on the test point the test pilot would apply maximum brakes or leave the aircraft rolling without brakes being applied. During a braked test run, maximum brakes were applied by the pilots just when the aircraft had entered the water pond (see Figure 20). Just before leaving the water pond the brakes would be released again (see Figure 20). Between each run sufficient time was taken for the brakes to cool down. Also the airframe and tyres were inspected for damages after each run. Video recordings and still images were made of each test run from the outside and inside the aircraft. These images were used in case water ingestion into the engines was suspected (see e.g. Figure 21). The videos and still images were also used in the post processing to analyse spray patterns for hydroplaning indications.




Future Sky Safety has received funding from the EU's Horizon 2020 Research and Innovation Programme, under Grant Agreement No. 640597.

# Typical run

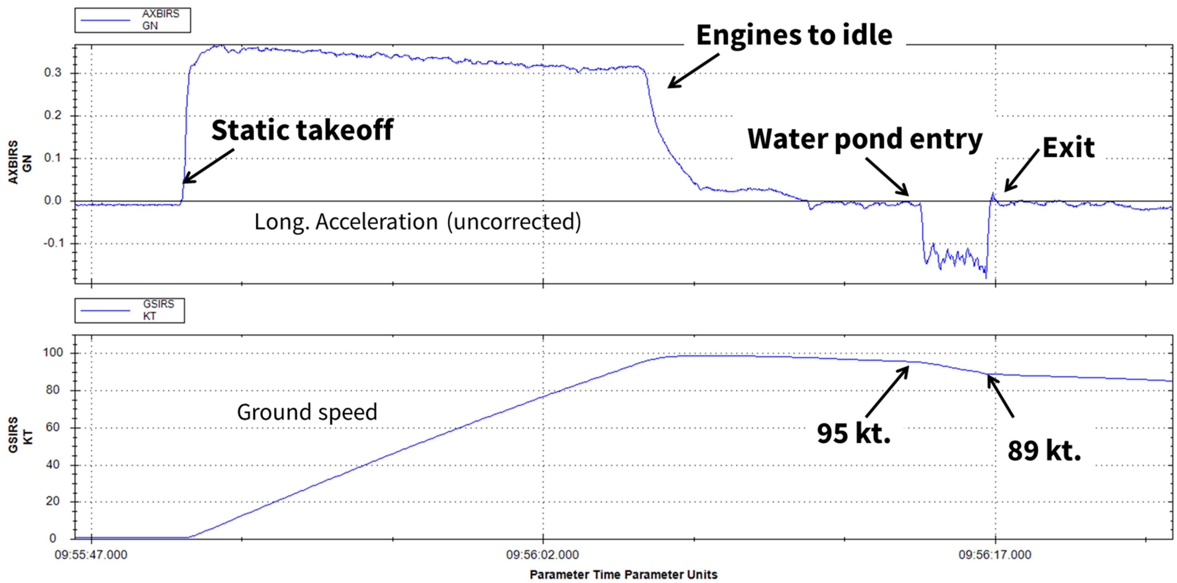


**Figure 19 Longitudinal acceleration and ground speed time-history plot for a typical test run.**

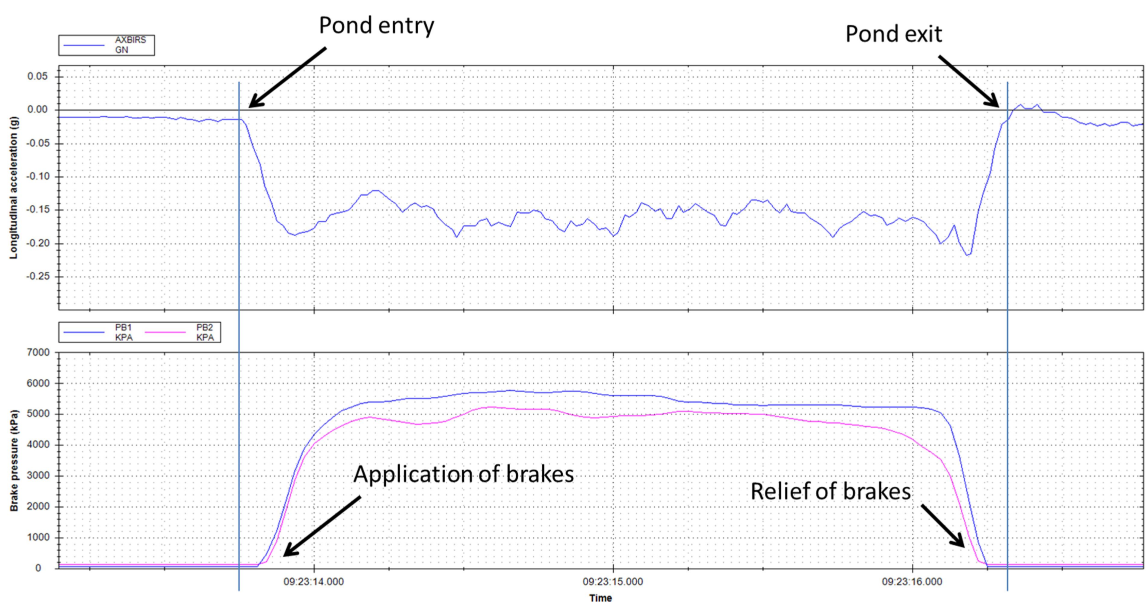


**Figure 20 Example time-history plot of longitudinal acceleration and brake pressure when running through the water pond (ground speed between 85-78 Kt.).**


**Figure 21 Cessna Citation test aircraft running through the water pond.**

## 3.2. Data Reduction and Analysis

Different parameters were recorded on board the test aircraft, including acceleration, airspeed, ground speed, engine parameters, brake pressures, and wheel speeds (see Table 3 for complete list) at (high) sample rates along with appropriate environmental measurements such as temperature, pressure, wind speed and direction. Weather data were taken from an official weather station that is located next to the runway. Weight and centre of gravity were determined before each test run. Water depth in the water pond was measured prior to each test run at 26 fixed locations. These locations were marked in the pond and corresponded to the lateral position of the main gear tyres. Uniformity in pilot brake application and proper aircraft configuration for a given series of test runs was determined from review of the time-history plots. The measured longitudinal acceleration was corrected for biases and pitch angle influence. The acceleration data were also smoothed using a special moving average algorithm.

The objective of this project is to establish the effective braking friction coefficient on a flooded runway as function of ground speed. The effective braking friction coefficient is defined by:

$$\mu_{EFF} = \frac{F_{Brake\_main}}{N_{main}}$$

This equation requires the braking force exerted on the main wheels and the normal load on the main wheels. As already noted, there are several forces acting on the aircraft when running through the water pond. From the aircraft performance database, information on aerodynamic drag, rolling friction and idle thrust can be obtained. However, the water layer also causes additional drag forces: tyre displacement drag and water impingement drag. From a braked run through the water pond it is not possible to differentiate between these last two forces and the main gear braking force. Therefore an unbraked run at nearly the same speed, weight and water depth as done for the braked run is needed. By subtracting the measured deceleration force of the unbraked test run from the measured deceleration force in the braked run, the braking friction force is obtained. This is illustrated below.

$$m_{braked}\, a_{braked} = T_{idle} - D_{aero} - F_{rolling} - D_{contamination} - F_{runway\ slope} - F_{Brake\_main}$$

$$-$$

$$m_{unbraked}\, a_{unbraked} = T_{idle} - D_{aero} - F_{rolling} - D_{contamination} - F_{runway\ slope}$$

$$=$$

$$m_{braked}\, a_{braked} - m_{unbraked}\, a_{unbraked} = -F_{Brake\_main}$$

With the recorded on board data , the normal load $N_{main}$ acting on the main gear tyres can be derived for the test aircraft using the force-moment diagram illustrated in Figure 22. For the derivation of the normal load, data on aerodynamics and engine thrust are also needed. Idle thrust data were obtained from the engine deck. Aerodynamic drag and lift data were obtained from Cessna. Data on pitching moments were estimated using data for a Cessna Citation 500.

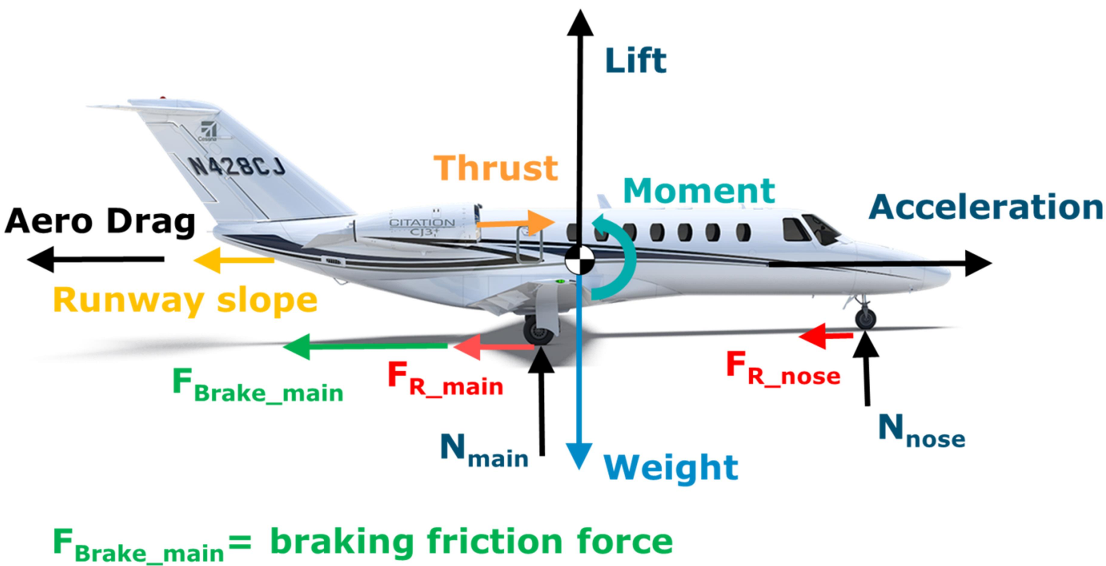


**Figure 22 Force diagram of a braked aircraft.**

**Table 3 Overview of parameters recorded on board as function of time.**

| Parameter | Sample rate |
|---|---|
| Normal acceleration, Lateral acceleration, and Longitudinal acceleration | 50 Hz |
| Groundspeed | 10-20 Hz |
| True airspeed | 8 Hz |
| Airspeed | 8Hz |
| Pilot commanded brake pressures | 20 Hz |
| Pitch angle | 50 Hz |
| Heading | 50 Hz |
| Left and right engine N1 | 20 Hz |
| Left and right engine N2 | 20 Hz |
| Elevator position | 64 Hz |
| Rudder | 64 Hz |
| Aileron | 64 Hz |
| Angle of attack | 50 Hz |
| Main wheel speeds | 50 Hz |
| Static temperature | 2 Hz |
| Static pressure | 2 Hz |
| Flap position | 20 Hz |
| Speed brake position | 20 Hz |
| Fuel mass flow Left engine | 20 Hz |
| Fuel mass flow Right engine | 20 Hz |




Future Sky Safety has received funding from the EU's Horizon 2020 Research and Innovation Programme, under Grant Agreement No. 640597.

## 3.3. Results and Discussion

### 3.1.7 Introduction

In this section the main results obtained from the flight tests data are presented. An example of data recorded is shown in Figure 23. This shows a number of recorded parameters from a few seconds before entering the water pond and after leaving the pond. The example also shows the corrected longitudinal acceleration as well as the longitudinal acceleration derived from the ground speed. As the ground speed was sampled at a high rate, differentiation of this speed leads to reasonable accurate normal acceleration data in the direction of travel (without having to correct it for pitch angle). This ground speed derived acceleration was used to cross check the directly measured (and corrected) longitudinal acceleration used for the analysis. During 2016 flight testing programme it was discovered that the wheel speed of the right main gear wheel was not recorded correctly in most of the runs (except for the last test run). This anomaly could not be fixed during the test programme. Only wheel speeds of the left main gear tyre could be used for analysis here. During the 2018 tests there were again some problems with the recording the right main gear wheel speeds.

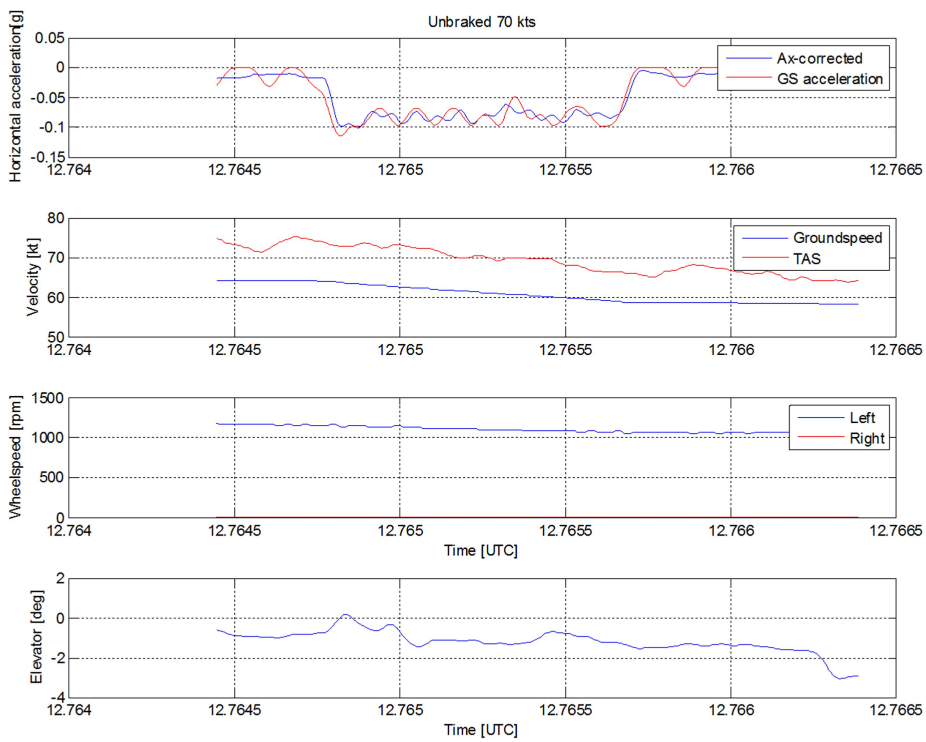


**Figure 23 Example of time-history plots.**




Future Sky Safety has received funding from the EU's Horizon 2020 Research and Innovation Programme, under Grant Agreement No. 640597.

### 3.1.8 Braking friction results

The effective braking friction coefficients derived from the test data are shown in Figure 24 as function of ground speed for two water depths. There is no large difference noticeable between the results for both water depths. As clearly illustrated the braking friction coefficient rapidly reduced as ground speed increases. Above 80 kt, only very low friction levels are found, similar to an icy runway. As part of a different project, the Cessna Citation was also tested on the same runway under wet conditions. The runway was artificially wetted for these tests. Water depths varied between 0.4-1.3 mm during these wet runway tests. Figure 25 shows a comparison between the wet and flooded runway (16.7 mm water depth) braking capabilities of a Cessna Citation II. The impact of the flooded runway on the braking capabilities is significant.

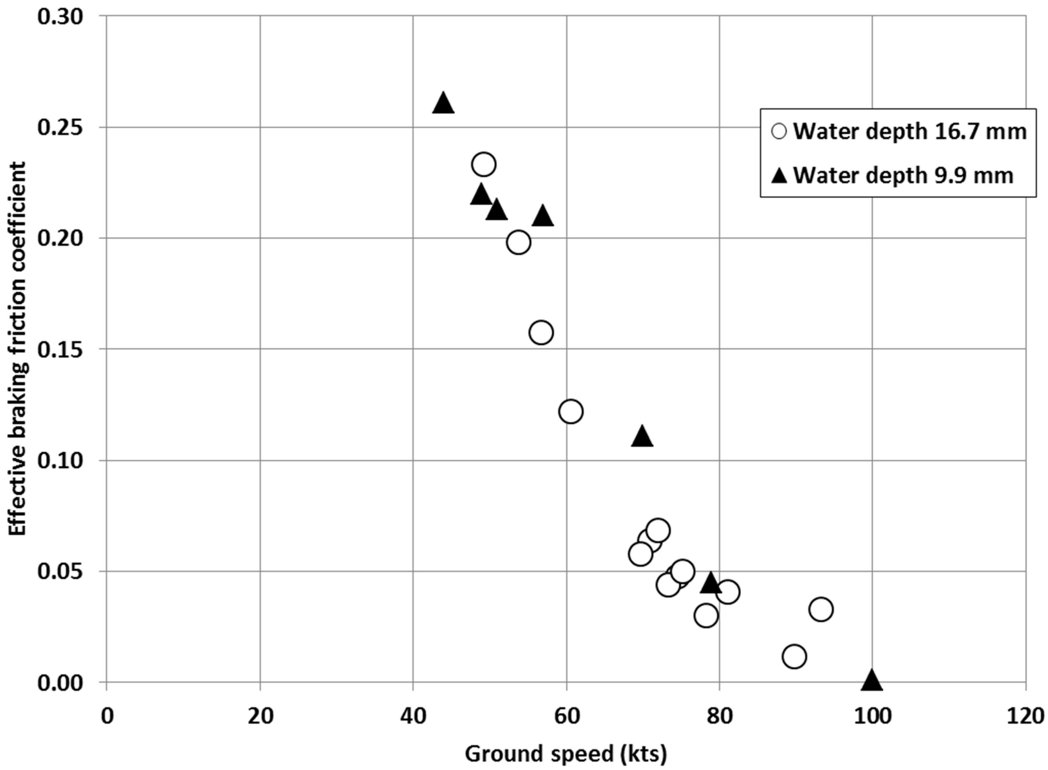


**Figure 24 Effective braking friction coefficient as function of ground speed for the Cessna Citation II on a flooded runway.**

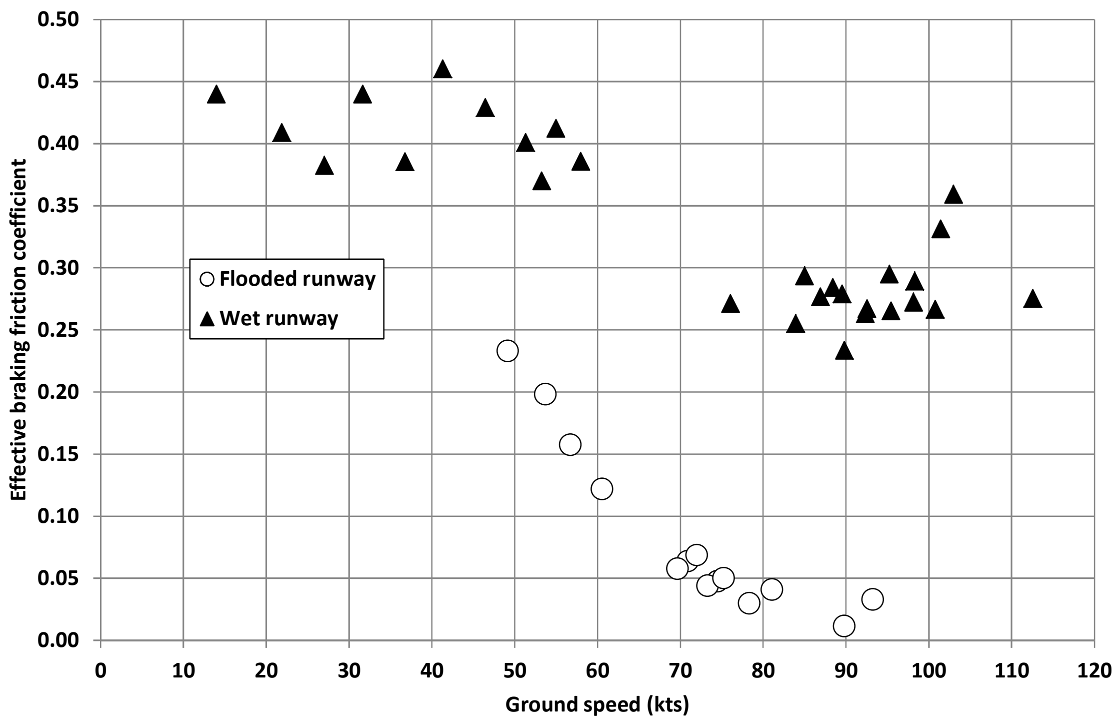


**Figure 25 Comparison of wet and flooded runway braking capabilities of a Cessna Citation II.**

### 3.1.9 Contamination drag main gear tyres

From the unbraked tests it is possible to derive the contamination drag due to the water displacement by the main gear tyres and impingement drag caused by the water spray generated by the main gear tyres. For this derivation the longitudinal acceleration just before the water pond entry and after exiting the water pond is subtracted from the longitudinal acceleration measured in the water pond. This acceleration is then multiplied with the aircraft mass to obtain the contamination drag. The derived contamination drag is compared to results obtained in an previous test programme (although at a lower water depth) and to a theoretical model provided by e.g. EASA AMC 25.1591. This model is presented here for completeness.

A tyre running through a layer of water/slush experiences additional drag due to the displacement of the fluid. This displacement drag is modelled using the analogy with aerodynamic drag and for a **single tire** is given by:

$$\mathbf{D_d = \frac{1}{2}\rho V_g^2 S C_{Ds} f_H}$$

$\rho$ = density of water or slush, $S$ = reference area, $C_{Ds}$ = displacement drag coefficient

$V_g$ = ground speed, $f_H$ = hydroplaning decay correction




Future Sky Safety has received funding from the EU's Horizon 2020 Research and Innovation Programme, under Grant Agreement No. 640597.

The reference area S in this equation is defined as: $S = d\, b_s$ with d being the water or slush depth and $b_s$ the tire width at fluid surface given as:

$$\mathbf{b_s = 2W\left[\frac{\delta + d}{W} - \left(\frac{\delta + d}{W}\right)^2\right]^{0.5} \ for \left(\frac{\delta + d}{W}\right) \leq 0.5}$$

W= tyre width (unloaded), $\delta$ = tyre vertical deflection (is a function of the normal load on the tyre and tyre inflation pressure amongst others)

For most aircraft tyres the drag coefficient $C_{Ds}$ varies between 0.70 and 0.80. An average of 0.75 is normally used (see EASA AMC 25.1591).

When the ground speed reaches the hydroplaning speed the displacement drag reduces. At this speed the tyre is separated from the runway by a water film. As the tyre is planning over a water film, less water is displaced and as a result the displacement drag reduces as speed increases beyond the hydroplaning speed. Different empirical formulae have been developed to account for this effect. Most of these formulae give very similar results. EASA AMC 25.1591 provides a graph showing the hydroplaning decay correction. This graph is also given by the following equation:

$$\mathbf{f_H = -0.54 + 7.24\left(\frac{V_g}{V_p}\right) - 8.01\left(\frac{V_g}{V_p}\right)^2 + 2.31\left(\frac{V_g}{V_p}\right)^3}$$

The (dynamic) hydroplaning speed is noted as $V_p$ in this equation and the ground speed by $V_g$. Vp of the main gear tyres is estimated from the test data to 90 Kt. (see section 3.1.10).

Figure 26 gives a comparison of the contamination drag for the main wheels derived in the present test programme to earlier tests conducted by NLR and EASA AMC 25.1591 model results. Note that the test aircraft in these previous tests had a slightly higher main gear tyre inflation pressure then in the present tests. The predicted contamination drag is somewhat lower than measured for both the 9.9 and 16.7 mm water depth cases. This is caused by the impingement drag. In particular the bow wave[1] causes additional drag from the forward spray hitting the airframe (mainly the wing in case of the Cessna Citation test aircraft, see Figure 27). The drag on the airframe by the forward spray depends upon where in the trajectory of the forward spray the aircraft catches up with the spray. If this occurs near the maximum height point of the trajectory then there would be a high impingement drag. However if this point is near the maximum forward point of the trajectory, hardly any impingement drag from the forward spray will be noticed.

[1] In front of the tyres a bow shaped wave front can develop at speeds greater than the surface wave as water builds up ahead of the tyre, ejecting a spray in forward and upward direction.

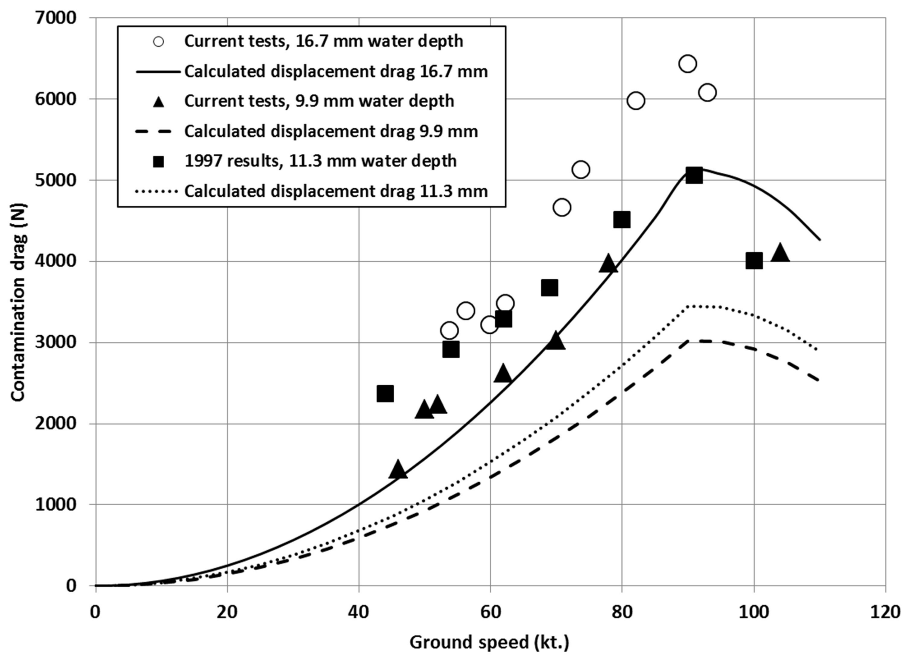


**Figure 26 Comparison of contamination drag derived in the present test programme to earlier tests and model results.**

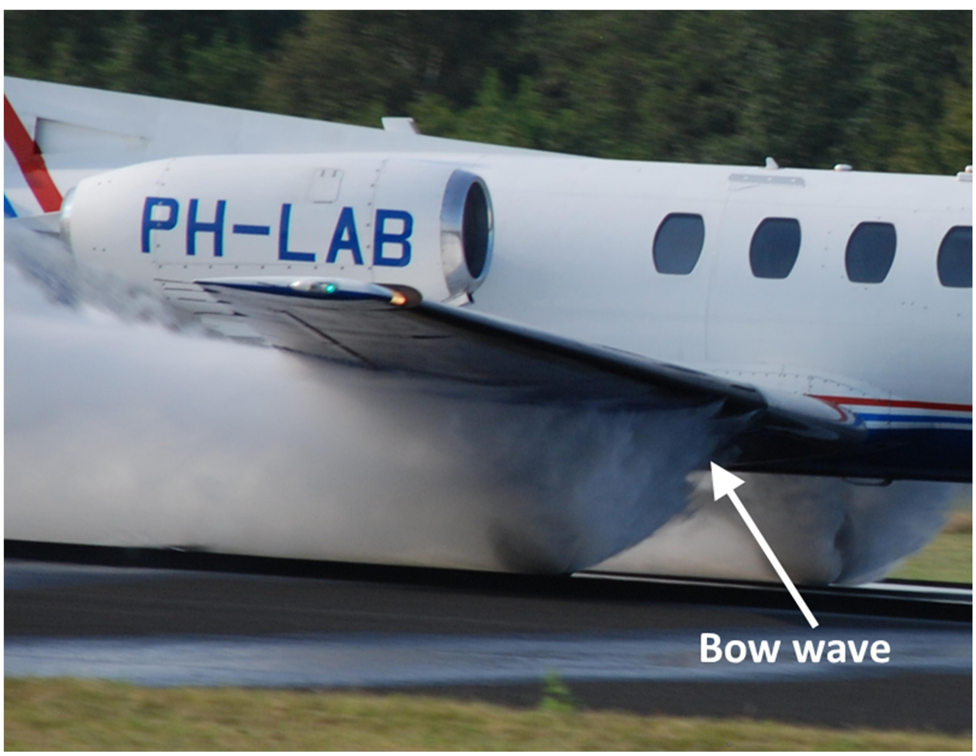


**Figure 27 Bow wave hitting the wing.**

### 3.1.10 Hydroplaning characteristics main gear tyres

Hydroplaning is defined as the condition under which the tyre footprint is lifted off from the water covered runway surface by the action of the fluid. The forces from the fluid pressures balance the vertical loading on the wheel. Since fluids cannot develop shear forces of a magnitude comparable with the forces developed during dry tyre-runway contact, tyre traction under this condition drops to values significantly lower than on a dry runway. Water pressures developed on the surface of the tyre footprint and on the ground surface beneath the footprint originate from the effects of either fluid density and/or fluid viscosity, depending upon conditions. This has resulted in the classification of hydroplaning into two types, namely dynamic and viscous hydroplaning. Considering the high water depths used in the present flight tests, dynamic hydroplaning will have a significant influence on the braking performance. The test runway surface has a harsh microtexture which limits the influence of viscous hydroplaning. The onset of full dynamic hydroplaning is not easy to determine. There are several manifestations of dynamic hydroplaning that can be observed from flight tests:

- Tyre bow wave suppression;
- Fluid drag peaks;
- Tyre spin-down.

These manifestations can be used to determine the dynamic hydroplaning speed of a tyre.

Experiments have shown progressive reduction of the bow wave spray angle as ground speed increases. Above the full (dynamic) hydroplaning speed the bow wave disappears completely. This information can be obtained from still photo images and videos recordings which are taken during the water ingestion tests. As the tyre reaches and exceeds the full hydroplaning speed, displacement and impingement drag start to reduce. The strongest indication of a full (dynamic) hydroplaning is the condition of unbraked wheels slowing down or stopping completely. The fluid dynamic lift force under the tyre causes the centre of pressure of vertical ground reaction to move ahead of the wheel axle with increasing ground speed. This causes a spin-down moment. At the hydroplaning speed this spin-down moment will exceed the total spin-up moment caused by all tyre drag forces. The tyre will start to spin-down and can come to a complete stop. Above the hydroplaning speed the centre of pressure of vertical ground reaction moves back to the wheel axle. As this time the tyre will start to spin-up again. As a rule of thumb the wheel speed should be less than 50% of that on a dry runway to have total dynamic hydroplaning. To analyse this wheel speed of the tyres need to be recorded during the flight tests. The wheel speed of the main gear tyres need to be related to the wheel speed obtained on a dry runway at the same ground speed. This relation can be obtained from the recorded wheel speeds prior to entering the water pond and just after exiting the water pond.

The still images taken during the test runs indicate that the bow wave is suppressed at higher ground speeds starting from 84 Kt. as shown in Figure 28. The bow wave is more or less flat at a speed of 92 Kt. This would suggest that the full hydroplaning speed is somewhere between 84 and 92 Kt. The contamination drag plot as function of ground speed (shown in Figure 26) suggests a peak in the drag at




Future Sky Safety has received funding from the EU's Horizon 2020 Research and Innovation Programme, under Grant Agreement No. 640597.

around 90 Kt. This plot only has a very few number of data points around this peak so this is not conclusive regarding the hydroplaning speed. Finally the wheel speed of the left main gear wheel is analysed. As noted the recording on the right main gear wheel were not useable. The minimum ratio between wheels speed in the water pond and the expected wheel speed on a dry surface as function of ground speed is shown in Figure 29. This plot shows that the wheel speed has drop below 50% of that on a dry runway at 92 Kt. ground speed (see also Figure 30). This would mean that full hydroplaning occurred below 92 Kt. but above 84 Kt. Although the number of data points are limited, Figure 29 suggests a hydroplaning speed of around 90 Kt.  Based on the above discussed data, the full (dynamic) hydroplaning speed is estimated to be 90 Kt. (ground speed). This also corresponds to the very low braking friction values shown in Figure 24 at and above this speed. It must be noted that determining hydroplaning speeds from flight test data is not an exact science even if all indicators for full dynamic hydroplaning are available. It remains a best estimate of the dynamic hydroplaning speed.




Future Sky Safety has received funding from the EU's Horizon 2020 Research and Innovation Programme, under Grant Agreement No. 640597.

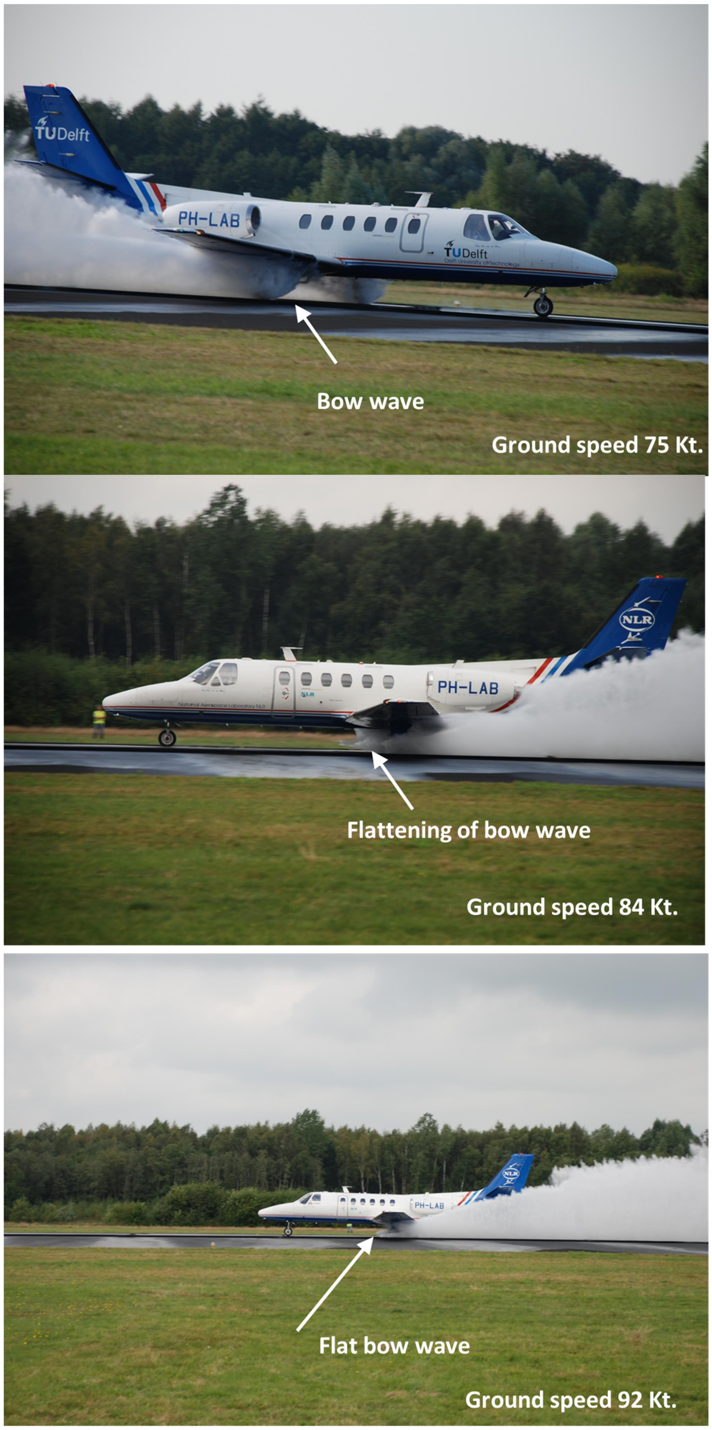


**Figure 28 Bow wave development.**




Future Sky Safety has received funding from the EU's Horizon 2020 Research and Innovation Programme, under Grant Agreement No. 640597.

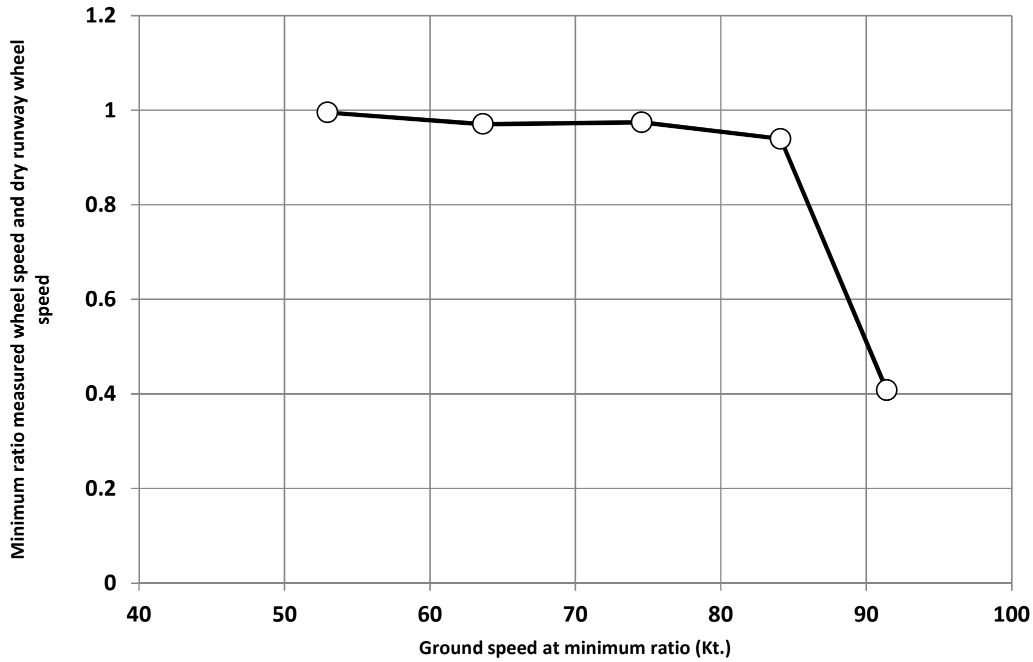


**Figure 29 Minimum ratio between wheels speed in water pond and expected wheels speed on a dry surface as function of ground speed.**

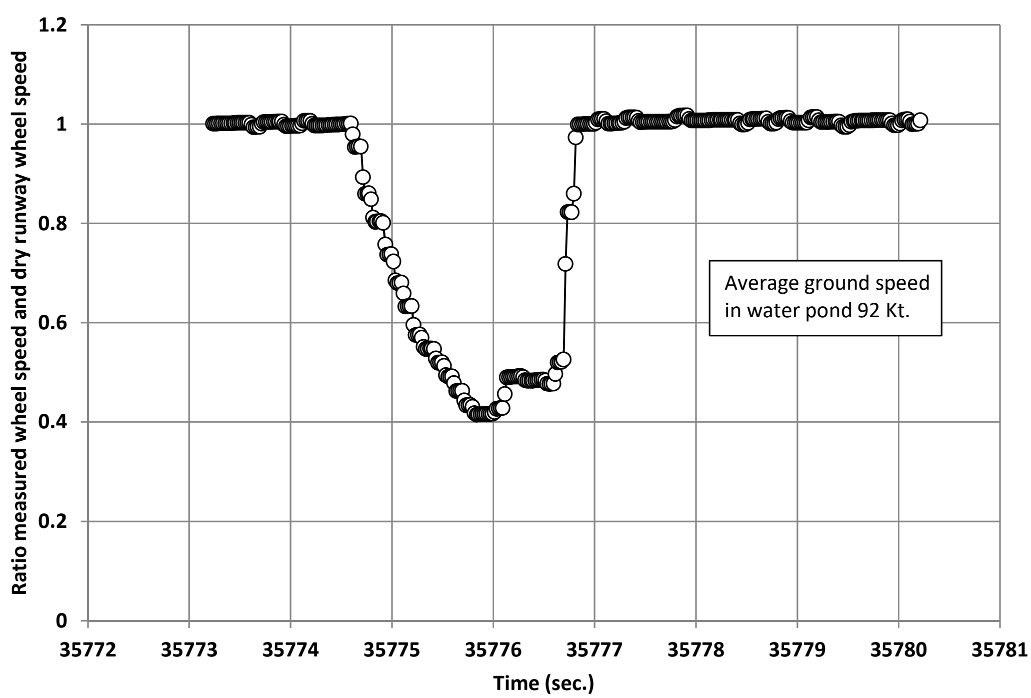


**Figure 30 Relative wheel speed left main gear tyre.**




Future Sky Safety has received funding from the EU's Horizon 2020 Research and Innovation Programme, under Grant Agreement No. 640597.

The wheel speeds were also recorded during the braked test runs through the water pond. Braked runs cannot be used to estimate the hydroplaning speed. However, they can provide insight in how the brake system functions in particular the anti-skid system. The anti-skid system is only active if the pilot meters a pressure in excess of that required to skid the tyre. The system then immediately reduces the braking level to minimise the depth and duration of the skid. This allows the wheel to spin back up, generating a reference speed for the anti-skid system. The antiskid then immediately allows braking to re-apply at a lower level. The pressure will be allowed to gradually increase again until either another skid occurs or the pilot's metered pressure is achieved. The anti-skid does not apply pressure on the brakes, but only relieves it. This whole process is conducted at a very high frequency (typically 200 Hz), allowing the anti-skid to react quickly to changes in runway slipperiness. When brakes are applied during severe tyre hydroplaning, the anti-skid system may lose its reference speed as the wheels are not spun up. The wheels remain locked up until the pilot releases the brake pedals. On some aircraft this problem is solved by using the groundspeed signals from the aircraft's inertial reference system as a backup wheel reference speed. On aircraft with a bogie main landing gear the rear wheels are used as a reference speed in preventing locked wheels conditions. The Cessna Citation II has a locked wheel crossover protection system installed. This prevents loss of aircraft control caused by unequal wheel rotation rates. When the anti-skid system detects that one main gear wheel is rotating 50% slower than the other, brake pressure to the slow wheel is dumped, allowing wheel speeds to equalise. The 50% tolerance between the wheel speeds is provided to permit an amount of differential braking, for steering purposes. Locked wheel crossover protection is functional at ground speeds greater than 40 knots. This level of protection is not available if both wheels are locked. The full hydroplaning speed of the main gear tyres was estimated to be 90 Kt. Just before this ground speed the wheels start to spin-down. If full brakes are then applied lockup of the wheels can occur. The locked wheel crossover protection system cannot prevent this from happening as the system will not detect that one main gear wheel is rotating 50% slower than the other as both are spinning down due to hydroplaning. This is illustrated in the wheel speed data shown in Figure 31 for ground speeds higher than the full hydroplaning speed. Just after entry of the water pond full brakes are applied. Immediately the wheel speeds drops to zero for both left and right main gear wheels[2]. Only after relieving of the brakes the wheels start turning again. At low ground speeds locked wheel conditions were not recorded.

[2] This was the only test run in which the wheels speeds were recorded for both left and right main gear.

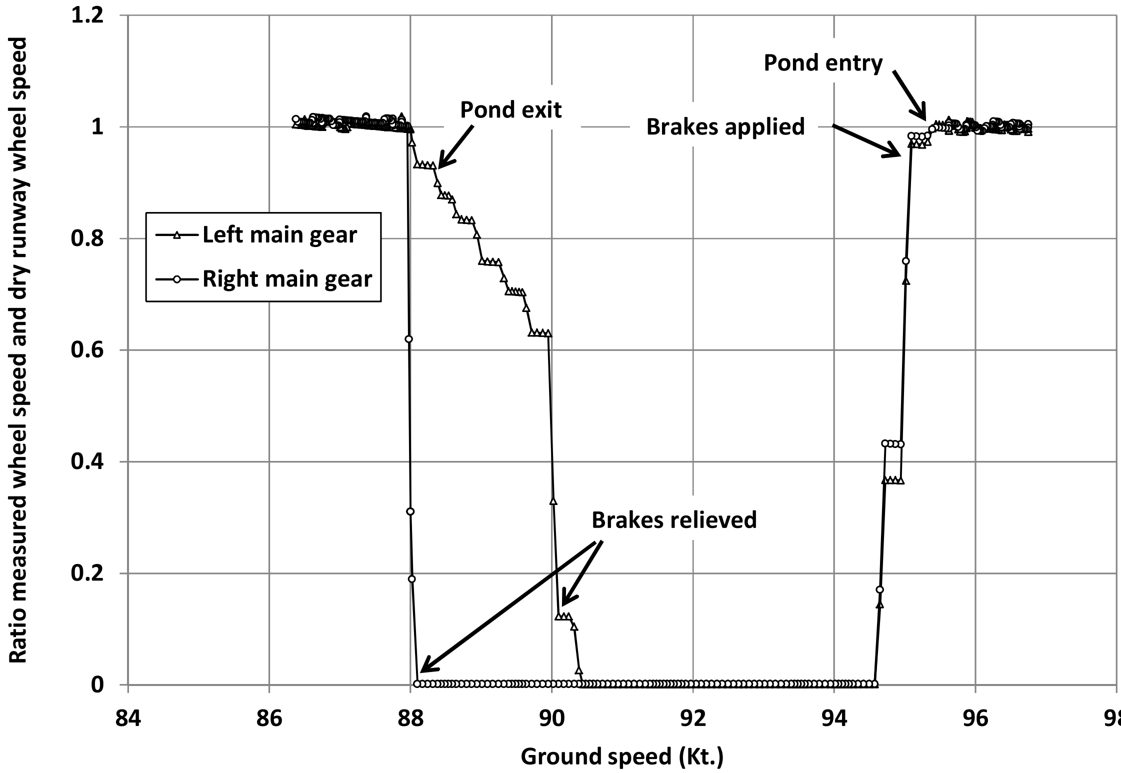


**Figure 31 Relative wheel speed as function of ground speed when running through the water pond in a braked condition.**

# 4 FLIGHT TEST RESULTS OBTAINED WITH A LARGE TRANSPORT AIRCRAFT

## 4.1. Test requirements

### 4.1.1 Test Objectives

The main objective of this flight test campaign is to evaluate the braking friction coefficient of an aircraft with state of the art tires and braking system on a contaminated runway. Secondarily, two additional aims have been outlined: displacement drag quantification and aquaplaning speed characterization. All these evaluations are to be performed at **tire** level.

A400M MSN002 was identified as appropriate for test purposes. The reasons behind this choice are not only the compliance it shows with the previously described requirements, but also the fact that it is fully instrumented, which allows for a more complete and precise data acquisition.

### 4.1.2 Test strategy

Considering the objectives presented in section 4.1.1, it is clear that one of the main targets of the analysis is to conveniently separate braking friction force and displacement drag from the remaining retarding force components acting on **a single tire**. As described in section 2, the retarding horizontal force has two components: one due to friction (caused by braking, deformation, or both), and another related to contaminant drag (displacement and impingement). These components cannot be isolated from one another in a single run. Therefore, this suggests the need for a specific testing methodology.

The flight test campaign was conceived as a series of test pairs, formed by an un-braked run and its braked back-to-back. Ideally, both tests would be conducted at exactly the same conditions in terms of aircraft configuration, aircraft weight, atmospheric conditions, ground speed and contaminant depth. Un-braked runs are useful for the identification of contaminant drag, whereas braked ones are, of course, necessary for the characterization of braking friction. The precise force identification methodology that was followed will be briefly described later in this section.

Moreover, considering that A400M is equipped with a multi-row MLG (triple tandem assembly), it is important to select which tires will be useful for the analysis. As can be expected, the analysis is to be focused on tires belonging to the **leading tandem row**. There are several reasons for this. First of all, front tires are responsible for displacing the vast majority of contaminant, leaving the runway in wet to dry conditions for the remaining rows (Ref. [3]). As a result, if operations in contaminated runways are to be properly characterized at tire level, only those tires actually subjected to contaminated conditions are to be taken into account. Besides, aft rows are subjected to contaminant impingement from forward tires. This constitutes an additional and undesired source of retarding force that is not to be characterized in this analysis.

Impingement drag is, indeed, a very important topic. European regulations (Ref. [1]) consider that the main contributor for this retarding force is fluid spray generated by the NLG. As already explained, all




Future Sky Safety has received funding from the EU's Horizon 2020 Research and Innovation Programme, under Grant Agreement No. 640597.

contributions that are not to be studied are to be minimized to the extent possible. In consequence, the designed runway was such that only MLG tires were affected by the contaminant, whereas NLG rolled over a dry surface.

With the following strategy in mind, an adequate separation of braking friction force and displacement drag is possible.

Displacement drag can be evaluated from un-braked tests results. At tire level, strain gauges installed on front wheels' axles provide direct measurements of the total horizontal (X) load each tire is subjected to. The components contributing to this load are contaminant (displacement) drag and rolling friction force. Once the latter is subtracted, a precise estimation of displacement drag will be obtained.

Braking friction is characterized by means of adequate treatment of brake torque pin measurements registered at braked runs.

The characterization of rolling friction (for its subtraction) is another important issue. As previously stated, it cannot be directly isolated from the remaining components of horizontal force. Nevertheless, its value can be estimated in two different ways:

1. Assuming a constant rolling friction of $\mu_{Roll} = 0.01$ (characteristic value for paved runways)
2. Performing some dry runs on the runway to be used for tests, in order to characterize rolling friction in a more precise manner.

The product of the selected $\mu_{Roll}$ by the normal force experimented by each tire can be regarded as a reasonably good estimation of the contribution of rolling friction to total retarding force.

Once a strategy for the isolation of retarding forces had been laid out, the next step was to define a methodology to test the influence of ground speed and water depth on these parameters.

Regulations (Ref.[1]) and literature (Ref.[2]) define braking friction as a function of **ground speed only**, with special considerations to be taken into account once aquaplaning speed has been reached. In terms of displacement drag, models (Ref. [2]) consider an important influence of both contaminant depth and ground speed. As a result, tests were focused on:

- Characterizing the influence of ground speed on braking friction, regarding depth as a correction parameter.
- Characterizing displacement drag as a function of both ground speed and contaminant depth.
- Additionally, estimating the minimum ground speed necessary for the onset of dynamic aquaplaning.

To sum up, the campaign was designed respecting the following three conditions:

- It should consist of a series of test pairs: an un-braked run, and its braked back-to-back.
- Each test pair was to be performed at a different ground speed, in order to allow for a precise characterization of braking friction as a function of this parameter.
- At least two remarkably different target depth values were to be used, in order to account for possible corrections in terms of contaminant depth.




Future Sky Safety has received funding from the EU's Horizon 2020 Research and Innovation Programme, under Grant Agreement No. 640597.

## 4.2. Test Means

### 4.1.3 Flight Test Aircraft

The aircraft chosen for testing was A400M MSN002. It is a military transport aircraft, equipped with four Europrop TP400 turboprop engines, as well as state-of-the-art landing gear and braking systems. Its test weight was approximately 110 t.

The main landing gear is attached to the left and right sides of the central fuselage. Each assembly is composed of three axles, each bearing two wheels. Each of the twelve tires of the MLG is identical. They follow a bias ply construction, and are inflated to a tire pressure of 138±5 psi. The dimensions of the tire are 43x15.5-17. The lateral spacing in each pair of wheels is 0.81m. The tires were neither new nor worn at the time of the testing, with groove depths between 10% to 90% of the allowable range.

Braking system, manufactured by Messier Bugatti, uses carbon brakes and includes a fully-modulating antiskid system, which is shared by each pair of wheels. Braking pressure is also common per pair of wheels on each axle. Therefore, only one wheel per tandem faces a potential friction limitation.

**Figure 32 Front view of A400M during the flight test campaign**

### 4.1.4 Test Facility

Flight tests were conducted at Twente Airport (EHTW), in the Netherlands. A former military base, it is currently employed for drone R&D, end-of-life aircraft recycling, local flight clubs and dedicated business aviation.




Future Sky Safety has received funding from the EU's Horizon 2020 Research and Innovation Programme, under Grant Agreement No. 640597.

Twente Airport is classified as Category B, and requires all operators to provide their flight crew with a previous briefing. The aerodrome was closed during testing, and FSS was granted exclusive use of its facilities during the campaign development. Due to the lack of Air Traffic Control means, dedicated airport control was supplied. Figure 33 shows a top-view of Twente Airport facilities.

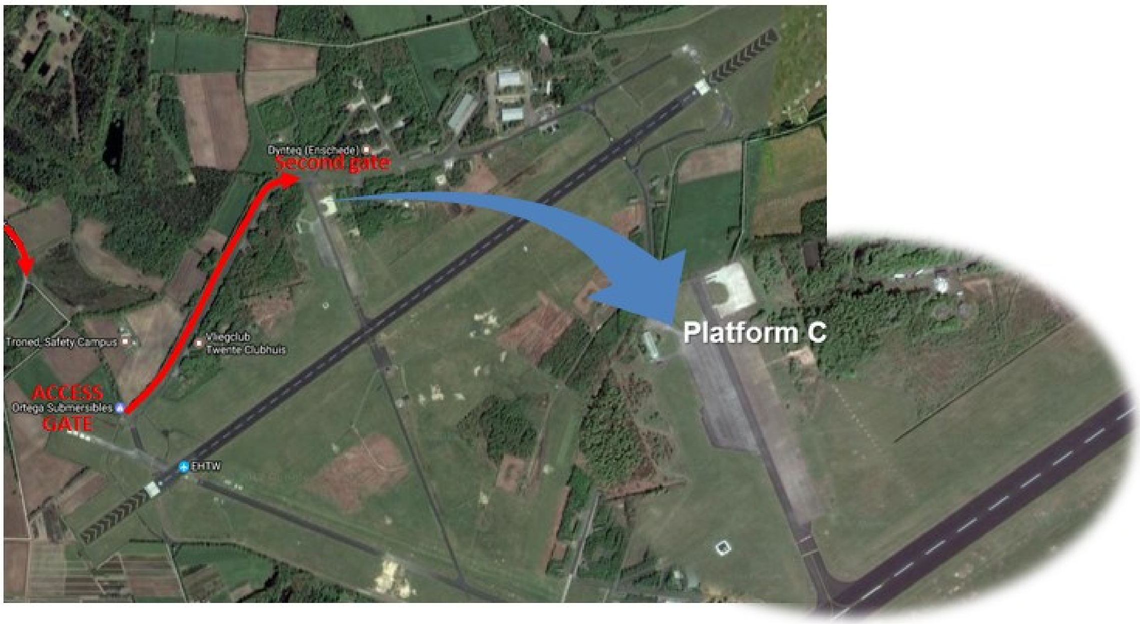


**Figure 33 Top view of Twente Airport facilities**

The runway selected for the flight test campaign was EHTW RWY 05/23, with a declared ASDA of 2406 m (plus additionally paved 300 m beyond each threshold), and a width of 45 m. Table 4 specifies the most representative runway distances.

| RWY | TORA (m) | TODA (m) | ASDA (m) | LDA (m) |
|---|---|---|---|---|
| 05 | 2406 | 2406 | 2406 | 2406 |
| 23 | 2406 | 2406 | 2406 | 2406 |

**Table 4 EHTW RWY 05/23 distances**

This runway presents two special features to aid braking performance, which are detailed below.

Firstly, both the runway surface and the additional paved zones are covered with a Possehl Antiskid top layer. This material presents an average macrotexture depth of 1.4 mm, and is intended to improve braking friction in wet conditions. Figure 34 shows an image of the Possehl material texture.

**Figure 34 Possehl texture**

In addition to this, and in order to aid water/fluid evacuation, the runway cross-section has a triangular-like shape. The transversal slope varies from 0.6-0.8% in the proximities of the centerline (within 5 m) to 1.5-1.6% at further distances. This feature is particularly advantageous in the context of this test campaign, since it allows the un-braked nose landing-gear to roll over a dry surface, so that only the main landing gear is affected by the contaminant.

### 4.1.5 Pond Construction

Experience gained from previous contaminated runway tests performed on Twente airport was crucial for the construction of the pond.

Figure 35 shows the specific position of the pond within RWY 05.




Future Sky Safety has received funding from the EU's Horizon 2020 Research and Innovation Programme, under Grant Agreement No. 640597.


**Figure 35 Top view of RWY 05, signalizing the position of the water pond**

As shown in Figure 36, the so-called “pond” consists, in fact, of two ponds, each 100 m long x 5 m wide, and located 1.15 m away from the runway centerline. The aim of this position was to permit the nose landing gear to roll over a dry surface, while the ponds are intended for the left and right sides of the main landing gear.

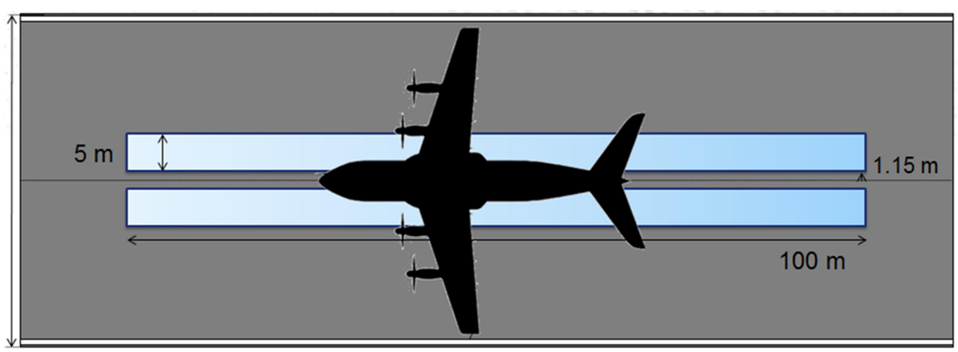


**Figure 36 Schematic representation of the pond disposition**




Future Sky Safety has received funding from the EU’s Horizon 2020 Research and Innovation Programme, under Grant Agreement No. 640597.

Since the NLG is not fitted with a brake, the fact that it is not affected by the contaminant will not affect braking friction results. Furthermore, the double-pond design presents two advantages:

- Impingement drag caused by the nose landing gear is avoided. This would constitute another undesired drag contribution, which would further complicate the calculation of braking friction in a contaminated medium.
- If the aircraft deviated from its track in the course of the run, additional controllability from nose wheels steering could be achieved.

Some other factors were also taken into account in the pond construction. An important one was that, due to the downward slope presented by the runway, water tended to accumulate at the exit of the pond. This made it difficult to maintain a uniform, target depth along the runway.

The solution found for this issue was to divide each pond in a series of sub-ponds along its length. As shown in Figure 37, 13 sections (each 7.7 m long) were considered. Although this design does not completely prevent the water from accumulating at the exit of each section, at least it allowed to keep a more uniform depth along the pond.

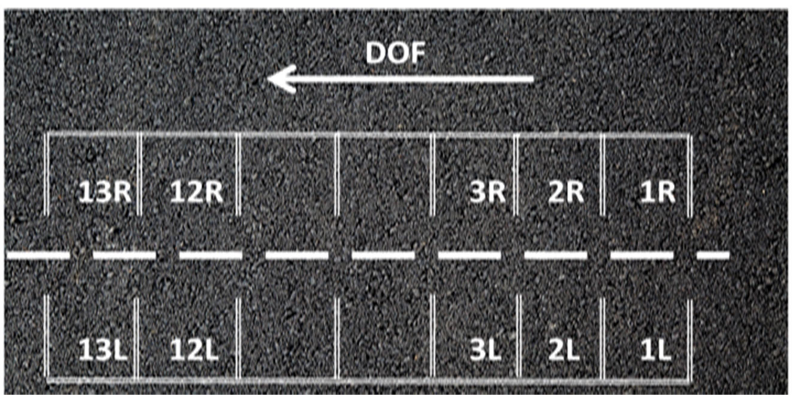


**Figure 37 Schematic representation of the 13 sub-divisions of the pond**

The establishment of several sub-ponds at each side, instead of a single one, serves an additional purpose: it diminishes the alterations in water ejection caused by the pass of the plane. That is, since sub-ponds are "isolated" from one another, the pass of the plane only has an effect on the water contained in the sub-pond where the plane is located in that instant, but not in the sub-ponds located either side. As a result, there is a reasonable agreement between the local depth values calculated from the initial measurements and those actually experienced by the front wheels.

The perimeters of both ponds, as well as the limits of the sub-ponds, were constructed using flexible rubber strips, inserted in grooves created in the runway surface (Figure 38). Water trucks were then employed to fill them to the required depth before each test run was conducted (Figure 39).




Future Sky Safety has received funding from the EU's Horizon 2020 Research and Innovation Programme, under Grant Agreement No. 640597.

**Figure 38 Detail view of the flexible rubber strips used to contain water within the pond**


**Figure 39 Water truck filling the pond before a flight test run**

A metal ring and a water depth gauge (Figure 40) were utilized to measure depths at two points in each sub-pond, 3.1 m away from the runway centerline at both left and right sides. This distance was chosen such that these are the lines over which the main landing gear wheels are expected to pass. The positions of the “measuring” points are specified in section 4.1.7.




Future Sky Safety has received funding from the EU’s Horizon 2020 Research and Innovation Programme, under Grant Agreement No. 640597.

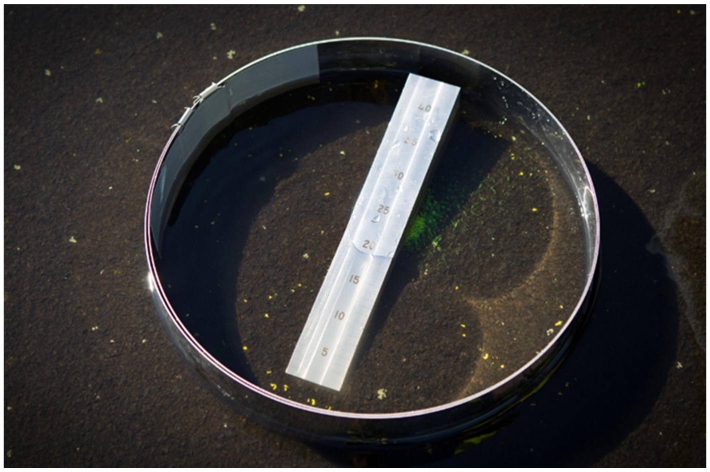

**Figure 40 Metal ring and water depth gauge, used for depth measurements**

These measurements serve two purposes. On the one hand, if they are significantly different from the target depth, they will give an indication to add or remove water. On the other hand, along with several hypotheses, they will allow to calculate water depth values at any position along the pond.

## 4.3. Flight Test Grid

Following the strategy outlined in section 4.1.2, the planned test grid comprised a total of **16 runs (8 test pairs)**, which aimed to cover a range of ground speeds between **60-110 kt**.

For flight safety reasons, it was decided to adopt a build-up approach in terms of speed, beginning with the lowest values of ground speed and increasing them gradually (by 10 kt) in each subsequent test pair.

Since depth is considered as a simple correction parameter for braking friction, 6 of the 8 planned test pairs were to be performed at the same target depth of **15 mm**. This is the same target depth selected in previous contaminated runway tests performed as part of FSS WP 3.2. These runs were intended to cover the complete speed range 60-110 kt.

Two test pairs were to be performed with a reduced target depth of **8 mm**. In this case, only a medium ground speed range (**80-90 kt**) was to be covered. The aim of these runs was not to establish a precise correlation, but to confirm, at a qualitative level, whether contaminant depth does not have an influence on effective braking friction (as established in CS-25 AMC 25.1591, Ref.[1]) or, on the contrary, its effect should be taken into account in performance calculations.

One of the most important constraints of the campaign definition is that runs comprising a single test pair should be performed in conditions as similar as possible. In order to achieve this, the plan was to perform them consecutively: first of all, the non-braked run, and then, the braked one. The time lapse between them should be as short as possible, comprising only the period necessary to refill the pond to its target depth and return the aircraft to a condition as similar as possible to that of the non-braked run. Reducing this interval will allow climatic conditions (temperature, humidity, and wind intensity and direction) to be as similar as possible in both runs.

Another requirement related with the previous constraint is that ground speed at the pond entry should be kept as similar as possible in the braked and non-braked runs belonging to the same pair.

The flight test grid is presented in the next two pages.




Future Sky Safety has received funding from the EU's Horizon 2020 Research and Innovation Programme, under Grant Agreement No. 640597.

**Table 5 Flight Test Grid**

| Test # | A/C weight | Flap configuration | Water pond entry speed GS (kts) | Brake application | Target Water depth | Aquaplaning risk |
|---|---|---|---|---|---|---|
| 1 | LOW to MED | 1 | 60 | Un-braked | 15 mm | No |
| 2 | LOW to MED | 1 | 60 | Maximum brake pedal | 15 mm | No |
| 3 | LOW to MED | 1 | 70 | Un-braked | 15 mm | No |
| 4 | LOW to MED | 1 | 70 | Maximum brake pedal | 15 mm | No |
| 5 | LOW to MED | 1 | 80 | Un-braked | 15 mm | No |
| 6 | LOW to MED | 1 | 80 | Maximum brake pedal | 15 mm | No |
| 7 | LOW to MED | 1 | 90 | Un-braked | 15 mm | Not expected but possible |
| 8 | LOW to MED | 1 | 90 | Maximum brake pedal[2] | 15 mm | Not expected but possible |
| 9 | LOW to MED | 1 | 100 | Un-braked | 15 mm | Expected |
| 10 | LOW to MED | 1 | 100 | Maximum brake pedal[2] | 15 mm | Expected |
| 11 | LOW to MED | 1 | 110 | Un-braked | 15 mm | Expected |
| 12 | LOW to MED | 1 | 110 | Maximum brake pedal[2] | 15 mm | Expected |

Flight Test Grid 2/2

| Test # | A/C weight | Flap configuration | Water pond entry speed GS (kts) | Brake application | Target Water depth | Aquaplaning risk |
|---|---|---|---|---|---|---|
| 13 | LOW to MED | 1 | 80 | Un-braked | 8 mm | No |
| 14 | LOW to MED | 1 | 80 | Maximum brake pedal | 8 mm | No |
| 15 | LOW to MED | 1 | 90 | Un-braked | 8 mm | Not expected but possible |
| 16 | LOW to MED | 1 | 90 | Maximum brake pedal[2] | 8 mm | Not expected but possible |

## 4.4. Theoretical Background

### 4.1.6 Test Runs

Table 6 shows the completed test grid. Tests R046 and R047 were performed on the first day of the campaign (21/03/2017), whereas tests R048 and R049 were completed on the second day (22/03/2017).

| Test run | Taxi | Test on taxi | Test point (FTR) | Avg. Ground speed [kt] | Brake application | Front row tire status W-C-A-M* | Test Validity |
|---|---|---|---|---|---|---|---|
| 1 | R046 | 1 | 3 | 67.5 | NO | [C C W C] | OK |
| 2 | R046 | 2 | 2 | 64.1 | YES | [C C C C] | OK |
| 3 | R047 | 1 | 5 | 79.1 | NO | [C C C C] | OK |
| 4 | R047 | 2 | 6 | 82.4 | YES | [C W C C] | OK |
| 5 | R047 | 3 | 7 | 92.1 | NO | [A C C C] | OK |
| 6 | R047 | 4 | 8 | 90.3 | YES | [A W C C] | OK |
| 7 | R048 | 1 | 9 | 102.0 | NO | [A W A A] | OK |
| 8 | R048 | 2 | 10 | 97.5 | YES | [A C A A] | OK |
| 9 | R048 | 3 | 11 | 112.0 | NO | [A W A A] | OK |
| 10 | R048 | 4 | 12 | 112.6 | YES | [A W A A] | OK |
| 11 | R049 | 1 | 1 | 58.2 | NO | [C C C C] | OK |
| 12 | R049 | 2 | 2 | 61.2 | YES | [M C C C] | OK |
| 13 | R049 | 3 | 15 | 93.0 | NO | [A W W C] | OK |
| 14 | R049 | 4 | 16 | 94.1 | YES | [A W W A] | OK |
| 15 | R049 | 5 | 13 | 77.4 | NO | [C W W C] | OK |
| 16 | R049 | 6 | 14 | 74.9 | YES | [M W C C] | OK |
| 17 | R049 | 7 | 4 | 69.2 | YES | [C C C C] | OK |

**Table 6 Completed Flight Test Grid**

* W= wet; C= Contaminated; A= Aquaplaning; M= Strong Anti-Skid modulation

Several items must be considered at this point. First of all, despite the initial plan to start with the lowest ground speeds (60 kt) and increase them progressively, the speed reached at the first run (R046_01, un-braked) was closer to a target of 70 kt. As a result, it was decided to continue increasing ground speeds in the subsequent tests, and perform the runs with a target speed of 60 kt (R049_01 and R049_02) on the second day.




Future Sky Safety has received funding from the EU's Horizon 2020 Research and Innovation Programme, under Grant Agreement No. 640597.

Secondly, the actually completed test grid consisted of 17 runs, one more than originally planned. Although R046_01 was deemed as representative for a target ground speed of 70 kt, its intended braked back-to-back (R046_02) was considered too slow for the newly intended target, and too fast for a target of 60 kt. As a result, it was decided to repeat it after all the test grid was completed (R049_07). Performing one run and its back-to-back on different days is not ideal, since climatic conditions may experiment slight variations. Nevertheless, the difference was not found to be significant to alter results substantially. In addition to this, had this run not been repeated, braking performance between 60 and 80 kt would have been poorly characterized.

## 4.5. Aircraft Monitored Data

Table 7 shows the main parameters measured and recorded digitally and controlled along the test.

**Table 7 Relevant measured parameters**

| Group | Parameter | Sample rate [Hz] |
|---|---|---|
| A/C kinematics | Normal, Lateral, and Longitudinal acceleration | 64 |
| | Ground speed | 64 |
| | True airspeed | 16 |
| | Wind speed | 16 |
| | DGPS | 4 |
| | Video camera on the aircraft belly | 24 |
| A/C angles | Pitch angle | 64 |
| | Angle of attack | 16 |
| | Heading | 64 |
| Atmosphere | Static temperature | 32 |
| | Static pressure | 8 |
| Powerplant | Powerplant power commanded | 4 |
| | Propeller torque | 8 |
| | Propeller RPM | 4 |
| | Calculated Net thrust | 4 |




Future Sky Safety has received funding from the EU's Horizon 2020 Research and Innovation Programme, under Grant Agreement No. 640597.

| | | |
|---|---|---|
| | Elevator | 128 |
| | Rudder | 128 |
| Control surfaces | Ailerons | 128 |
| | Spoiler deflection | 64 |
| | Flap position | 16 |
| | Wheel speed (12 wheels) | 32 |
| | Shock Absorber Stroke (6 legs) | 256 |
| | Brake torque pin (12 wheels) | 128 |
| | NLG Horizontal force per wheel (2 wheels) | 128 |
| LG system | NLG Vertical force per wheel (2 wheels) | 128 |
| | MLG Horizontal force per wheel (12 wheels) | 128 |
| | MLG Vertical force per wheel (12 wheels) | 128 |
| | Brake pressure (6 circuits) | 128 |
| | Brake pedal deflection (left/right) | 8 |

In addition to this, tire pressure was manually controlled each day in the campaign. Table 8 below shows the measured data on the four front wheels. The numbering of the wheels is shown in Figure 41.

| Wheel number | Inflation Pressure | |
|---|---|---|
| | Taxis R46, R47 | Taxis R48,R49 |
| 1 | 140 | 140 |
| 2 | 141 | 143 |
| 3 | 140 | 142 |
| 4 | 141 | 142 |

**Table 8 Inflation pressures on front axle wheels (1 to 4)**




Future Sky Safety has received funding from the EU's Horizon 2020 Research and Innovation Programme, under Grant Agreement No. 640597.

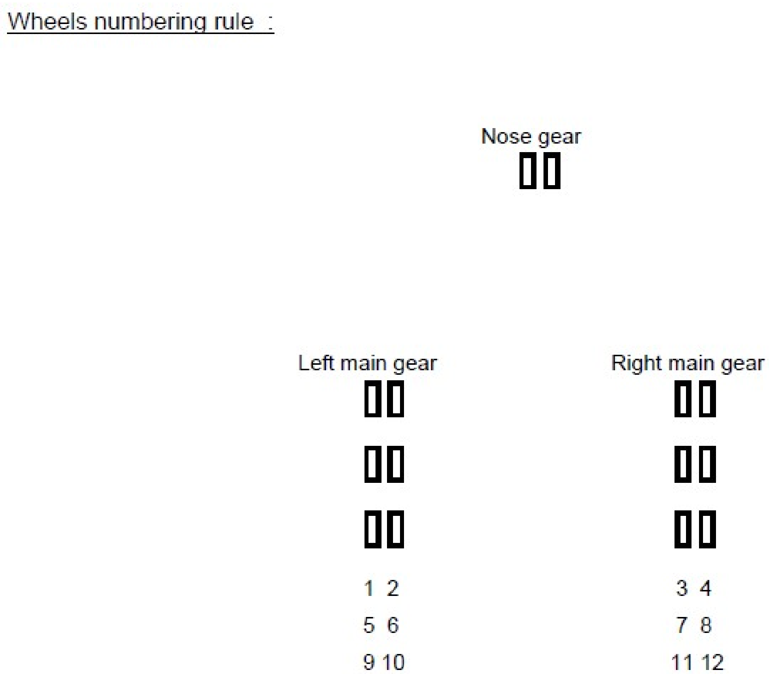


**Figure 41 Landing gear wheels denomination**

Tire pressures were not adjusted in the campaign. The second day testing (R048 and R049) the ambient static temperature was warmer than the first day. Because of this the tire pressure rose around 1-2 psi.

## 4.6. Water pond data

### 4.1.7 Depth estimation

One of the main difficulties for test data analysis is the longitudinal and transversal variation of contaminant depth. The runway shape caused water to accumulate at the exit of each sub-pond (due to the slight downward slope), as well as at the outer side of the pond (due to the transversal slope). As a result, it can be expected that inner wheels will encounter lower depth values than outer wheels.

Although a target depth was established for each test, this should be considered only as an illustrative value. It may be representative for the average depth of the complete pond or each of its 13 divisions, but by no means for local depth values.

It must also be taken into account that the left and right landing gears roll over separate pools, so they may encounter different depth values.

As a result, adequate measurement and calculation of water depth constitutes a crucial issue, if a relationship between contaminant depth and braking friction is to be established.




Future Sky Safety has received funding from the EU's Horizon 2020 Research and Innovation Programme, under Grant Agreement No. 640597.

This section is dedicated to explaining the method selected for measuring local water depths, as well as the assumptions and calculations made in order to estimate depth values at any point within the pond.

#### 4.1.7.1 Pond Depth Measurements

Water depth has been measured at two points of each subdivision of the pond. The position of these points is detailed in Figure 42: 3.1 m away from the runway centerline, and each at 2.5 m from the initial and final limits of the sub-pond. As previously stated, these are representative depth measurements in the line along which it is expected that the main landing gear wheels will run.

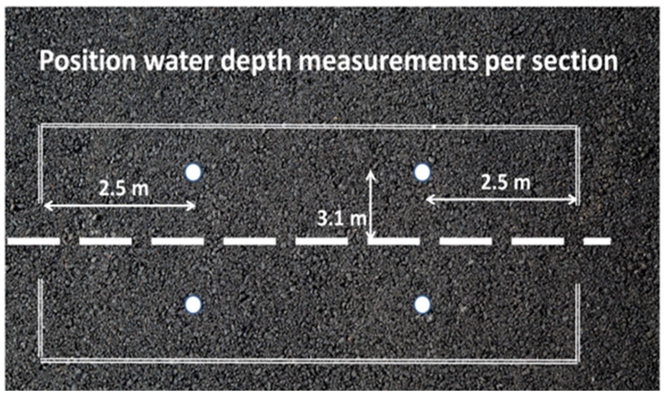


**Figure 42 Position of points designed for depth measurements**

Taking into account that each subdivision is 7.7 m long, the distance between two points belonging to the same pond is 2.7 m. Since there are 13 subdivisions at each side of the runway centerline, this makes a total of 52 point measurements.

#### 4.1.7.2 Assumptions

Local variations of water depth have been calculated individually for each of the 26 sub-ponds (13 at each side of the centerline). In order to do this, three important assumptions were made:

1. Denoting depths measured in each sub-pond as $D_1$ and $D_2$, the average of these values, $D_{av} = \frac{D_1+D_2}{2}$ is assumed to be the depth found at the point located in between measurement points 1 and 2. As a reminder, this "middle" point is located 3.1 m away from the inner side of the pond, and 3.85 m away from both the entry and exit ends of each sub-pond.

2. Transversal slope inside the pond is assumed to be constant, and equal to the average transversal slope. This yields a value of 1.33% at each side of the centerline.




Future Sky Safety has received funding from the EU's Horizon 2020 Research and Innovation Programme, under Grant Agreement No. 640597.

3. Longitudinal slope inside the pond is assumed to be constant inside each pond, but changes between one pond and another are taken into account. It is calculated as $\mathrm{slope_i} = \frac{\mathrm{D_1+D_2}}{\mathrm{L}}$, where

    - $\mathrm{slope}_i$ represents the slope of each sub-pond i=1 to 13.
    - $D_1$ and $D_2$ represent depth measurements at the two points selected at each sub-pond
    - L represents distance between these points.

4. Limits between sub-ponds will be treated as discontinuities. In other words, depth calculations will be conducted individually at each sub-pond.

5. Water depth in each sub-pond is assumed to vary in a uniform manner, both transversally and longitudinally.

Although the fifth assumption may seem obvious, it has been considered important to remark it. Since depth is assumed to vary uniformly, and no restrictions have been imposed, the calculation may yield negative depth values at some points. Since this is physically impossible, it leads to the following final assumption:

6. If, at any point, depth calculation yields a negative value, this result will be discarded and substituted by a zero.

#### *4.1.7.3 Pond Depth Calculations*

As stated previously, depth is calculated individually in each sub-pond, based upon two depth measurements and several simplifying assumptions.

For simplicity:

- x denotes the longitudinal direction of the **runway**, considered positive from pond entry to pond exit.
- y denotes the transversal direction of the **pond,** regarded as positive when directed towards the outer side of the pond.

A two-step extrapolation process is followed, as described below.

1. Firstly, taking into account:
    - Assumed depth, $Di_{av}$, at the “middle” point of each sub-pond (located at 3.1 m away from the inner side of the pond, and 3.85 m away from each end of the sub-pond)
    - Assumed constant longitudinal slope at each sub-pond $\mathrm{slope}_i$

Local water depth values are calculated at the line

- Parallel to runway axis
- Located 3.1 m away from the inner side of the pond




Future Sky Safety has received funding from the EU’s Horizon 2020 Research and Innovation Programme, under Grant Agreement No. 640597.

Considering x=0.0 m at the left end of the sub-pond, and x=7.70 m at the right end, depth, denoted by Di $_{3.1m}$ is given by:

$$\boldsymbol{Di}_{\ 3.1m}(\boldsymbol{x}) = \boldsymbol{Di}_{av} + \boldsymbol{slope}_i * (\boldsymbol{x} - \mathbf{3.85}) * \mathbf{1000} \quad \text{(Eq. 1)}$$

In this formula, x is expressed in m, and water depth in mm.

2. Using the depth calculations from the previous step, as well as the assumed constant transversal slope of 1.33%, depth values are now transversally extrapolated.

   Considering
   - y=0.0 m at the inner side of the pond, and y=5.0 m at the outer side of the pond
   - $Di_{3.1m}(x)$ as a known value from the previous step:

$$\boldsymbol{Di}(\boldsymbol{x}, \boldsymbol{y}) = \boldsymbol{Di}_{3.1m}(\boldsymbol{x}) + \mathbf{0.0133} * (\boldsymbol{y} - \mathbf{3.1}) * \mathbf{1000} \quad \text{(Eq. 2)}$$

In this formula, y is expressed in m, and water depth in mm.

Globally, water depth (mm) at any position (x,y) inside each sub-pond is given by:

$$\boldsymbol{Di}(\boldsymbol{x}, \boldsymbol{y}) = \boldsymbol{Di}_{av} + \boldsymbol{slope}_i * (\boldsymbol{x} - \mathbf{3.85}) * \mathbf{1000} + \mathbf{0.0133} * (\boldsymbol{y} - \mathbf{3.1}) * \mathbf{1000} \quad \text{(Eq. 3)}$$

As previously stated, if this formula provides a negative depth value, this should be immediately discarded and substituted by a zero.

#### *4.1.7.4 Additional Remarks*

The previously described process constitutes the basis for the depth calculations at each run. Due to the longitudinal and transversal slopes of the runway, a precise local characterization of the pond is an essential task.

At this point, three remarks are important. First of all, since the ponds are refilled and their representative depths measured before each run, depth will vary from run to run. Consequently, one depth calculation per run was required.

Secondly, as previously stated, main landing gear traces were expected to go over the 3.1m lines at each side of the runway axis. Nevertheless, the aircraft was likely to experience moderate lateral deviations from its desired trajectory, which must be taken into account, due to the important local variations in water depth. As a result, adequate tracking of wheel positions along each run was essential for an adequate data reduction and analysis.




Future Sky Safety has received funding from the EU's Horizon 2020 Research and Innovation Programme, under Grant Agreement No. 640597.

The third and final consideration was related to A400M MLG configuration. Unlike Cessna Citation II (used in previous NLR tests), which was equipped with a single row of twin-tires at each side of the fuselage, A400M has a three row MLG, also with twin tires at each side. The first row will displace a major amount of the water present in the runway. As a result, it will only be possible to make a correlation between contaminant depth and individual tire behavior for tires belonging to the first row. For the remaining ones, depth values will be unknown and impossible to calculate or estimate. Hence data for the first row shall only be included in this report

### 4.1.8 Water Pond Depth Per Test Run

Table 9 shows the registered values of the water depth gauges for each test run.

Following the methodology described in section 4.2.1, a map of water depths as a function of x and y pond coordinates was built for each test run. Figure 43 shows the depth map corresponding to test run 17 (R049_06).

Contaminated area is colored in different shades of blue; darker zones represent higher contaminant depths and vice-versa. Grey areas represent zones in which water depth is lower than 3 mm; as a result, they are regarded as wet, instead of contaminated. The dry central area designed for the NLG is represented in white.

Desired (green dashed lines) and actual (solid red lines) aircraft trajectories are also represented. As explained in Section 4.2.1, aircraft centerlines of each MLG side were expected to go over lines located 3.1 m away of the runway centerline. In other words, the aircraft was ideally expected to be perfectly centered in the runway. Nevertheless, due to the unavoidable aircraft lateral deviation at the time of performing the tests, real trajectories differed slightly from the initially intended ones.




Future Sky Safety has received funding from the EU's Horizon 2020 Research and Innovation Programme, under Grant Agreement No. 640597.

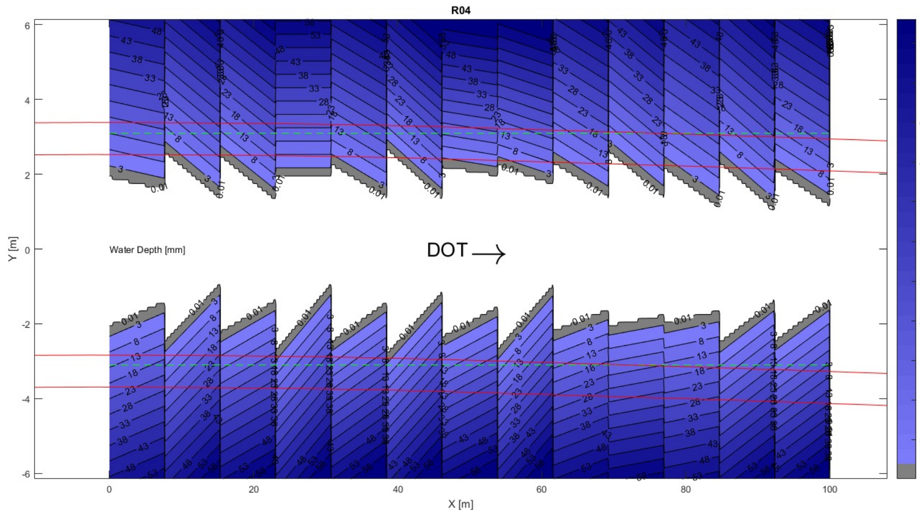


**Figure 43 Depth map of test run 17 (R049_06)**

Due to this lateral deviation, and the considerable transversal slope of the runway (1.33% at each side of the runway), it is rather straightforward to conclude that depths faced by each of the four frontal tires may be very different in a single test run.

This condition presented a constraint, since it introduced an additional source of complexity in the subsequent analysis. However, when observing the MLG loads signal, sampled at 128Hz, it was not possible to appreciate neither the evolution of the measurement with the water depth transitions nor the jumps from sub-pond to sub-pond. On the contrary, measurements were in general smooth and relatively constant, coherent with the small decrease in ground speed and the average value of water depth across the tire track.




Future Sky Safety has received funding from the EU's Horizon 2020 Research and Innovation Programme, under Grant Agreement No. 640597.

**Table 9 Registered values of the water depth gauges for each test run**

| RUN | SIDE | X POSITION ON THE WATER POND | | | | | | | | | | | | | | | | | | | | | | | | | |
|---|---|---|---|---|---|---|---|---|---|---|---|---|---|---|---|---|---|---|---|---|---|---|---|---|---|---|---|
| | | 2.5 | 5.2 | 10.2 | 12.9 | 17.9 | 20.6 | 25.6 | 28.3 | 33.3 | 36 | 41 | 43.7 | 48.7 | 51.4 | 56.4 | 59.1 | 64.1 | 66.8 | 71.8 | 74.5 | 79.5 | 82.2 | 87.2 | 89.9 | 94.9 | 97.6 |
| 1 | Right | 15.0 | 15.0 | 16.0 | 14.0 | 17.0 | 16.0 | 16.0 | 15.0 | 16.0 | 14.0 | 10.0 | 7.0 | 15.0 | 13.0 | 17.0 | 13.0 | 16.0 | 14.0 | 15.0 | 13.0 | 15.0 | 14.0 | 14.0 | 15.0 | 13.0 | 13.0 |
| | Left | 16.0 | 13.0 | 19.0 | 16.0 | 17.0 | 12.0 | 20.0 | 17.0 | 20.0 | 15.0 | 20.0 | 14.0 | 20.0 | 17.0 | 19.0 | 13.0 | 13.0 | 11.0 | 18.0 | 17.0 | 20.0 | 14.0 | 13.0 | 11.0 | 15.0 | 11.0 |
| 2 | Right | 14.0 | 15.0 | 18.0 | 16.0 | 17.0 | 17.0 | 18.0 | 16.0 | 18.0 | 16.0 | 18.0 | 15.0 | 18.0 | 15.0 | 17.0 | 15.0 | 16.0 | 14.0 | 17.0 | 15.0 | 17.0 | 15.0 | 17.0 | 17.0 | 19.0 | 17.0 |
| | Left | 16.0 | 12.0 | 19.0 | 17.0 | 15.0 | 13.0 | 19.0 | 14.0 | 18.0 | 13.0 | 20.0 | 15.0 | 18.0 | 13.0 | 19.0 | 15.0 | 20.0 | 17.0 | 18.0 | 17.0 | 22.0 | 15.0 | 19.0 | 17.0 | 19.0 | 16.0 |
| 3 | Right | 15.0 | 14.0 | 19.0 | 15.0 | 15.0 | 14.0 | 16.0 | 15.0 | 13.0 | 11.0 | 17.0 | 15.0 | 14.0 | 11.0 | 16.0 | 13.0 | 18.0 | 16.0 | 19.0 | 16.0 | | | 17.0 | 17.0 | 15.0 | 16.0 |
| | Left | 15.0 | 12.0 | 17.0 | 15.0 | 11.0 | 10.0 | 17.0 | 14.0 | 19.0 | 14.0 | 20.0 | 14.0 | 17.0 | 12.0 | 17.0 | 12.0 | 18.0 | 15.0 | 19.0 | 17.0 | 21.0 | 14.0 | 18.0 | 15.0 | 18.0 | 17.0 |
| 4 | Right | 19.0 | 17.0 | 18.0 | 13.0 | 19.0 | 17.0 | 19.0 | 17.0 | 19.0 | 16.0 | 19.0 | 16.0 | 19.0 | 16.0 | 20.0 | 16.0 | 19.0 | 17.0 | 19.0 | 15.0 | 18.0 | 16.0 | 17.0 | 17.0 | 20.0 | 18.0 |
| | Left | 15.0 | 10.0 | 20.0 | 17.0 | 16.0 | 13.0 | 19.0 | 14.0 | 18.0 | 13.0 | 20.0 | 14.0 | 17.0 | 11.0 | 17.0 | 13.0 | 19.0 | 16.0 | 19.0 | 17.0 | 17.0 | 14.0 | 18.0 | 15.0 | 18.0 | 16.0 |
| 5 | Right | 14.0 | 13.0 | 16.0 | 12.0 | 16.0 | 15.0 | 17.0 | 15.0 | 17.0 | 15.0 | 19.0 | 18.0 | 18.0 | 15.0 | 17.0 | 15.0 | 18.0 | 15.0 | 18.0 | 14.0 | 15.0 | 12.0 | 19.0 | 18.0 | 14.0 | 15.0 |
| | Left | 16.0 | 16.0 | 18.0 | 14.0 | 18.0 | 13.0 | 17.0 | 13.0 | 18.0 | 14.0 | 18.0 | 12.0 | 18.0 | 12.0 | 20.0 | 15.0 | 17.0 | 16.0 | 16.0 | 15.0 | 21.0 | 15.0 | 19.0 | 15.0 | 19.0 | 17.0 |
| 6 | Right | 16.0 | 15.0 | 19.0 | 17.0 | 17.0 | 16.0 | 19.0 | 17.0 | 19.0 | 18.0 | 19.0 | 17.0 | 19.0 | 19.0 | 19.0 | 15.0 | 19.0 | 18.0 | 19.0 | 18.0 | 17.0 | 15.0 | 19.0 | 19.0 | 20.0 | 19.0 |
| | Left | 17.0 | 14.0 | 18.0 | 15.0 | 19.0 | 16.0 | 18.0 | 14.0 | 19.0 | 15.0 | 18.0 | 13.0 | 20.0 | 16.0 | 19.0 | 14.0 | 17.0 | 14.0 | 19.0 | 16.0 | 20.0 | 15.0 | 18.0 | 16.0 | 17.0 | 15.0 |
| 7 | Right | 18.0 | 17.0 | 16.0 | 14.0 | 15.0 | 14.0 | 18.0 | 16.0 | 18.0 | 16.0 | 17.0 | 15.0 | 17.0 | 15.0 | 17.0 | 16.0 | 17.0 | 15.0 | 17.0 | 14.0 | 17.0 | 15.0 | 19.0 | 18.0 | 18.0 | 16.0 |
| | Left | 18.0 | 15.0 | 16.0 | 12.0 | 19.0 | 16.0 | 17.0 | 11.0 | 16.0 | 12.0 | 16.0 | 11.0 | 18.0 | 11.0 | 18.0 | 10.0 | 19.0 | 16.0 | 16.0 | 14.0 | 17.0 | 15.0 | 20.0 | 16.0 | 19.0 | 17.0 |
| 8 | Right | 16.0 | 15.0 | 19.0 | 17.0 | 16.0 | 16.0 | 19.0 | 16.0 | 17.0 | 15.0 | 16.0 | 13.0 | 19.0 | 17.0 | 19.0 | 17.0 | 19.0 | 17.0 | 16.0 | 13.0 | 17.0 | 15.0 | 17.0 | 16.0 | 16.0 | 15.0 |
| | Left | 19.0 | 15.0 | 17.0 | 14.0 | 14.0 | 11.0 | 18.0 | 13.0 | 19.0 | 15.0 | 19.0 | 15.0 | 19.0 | 14.0 | 16.0 | 12.0 | 16.0 | 13.0 | 20.0 | 16.0 | 19.0 | 16.0 | 19.0 | 15.0 | 15.0 | 13.0 |
| 9 | Right | 19.0 | 17.0 | 19.0 | 16.0 | 15.0 | 13.0 | 19.0 | 17.0 | 19.0 | 17.0 | 19.0 | 17.0 | 19.0 | 17.0 | 19.0 | 17.0 | 19.0 | 17.0 | 19.0 | 17.0 | 19.0 | 17.0 | 16.0 | 17.0 | 16.0 | 16.0 |
| | Left | 18.0 | 15.0 | 16.0 | 12.0 | 17.0 | 13.0 | 19.0 | 14.0 | 19.0 | 15.0 | 20.0 | 15.0 | 21.0 | 15.0 | 17.0 | 12.0 | 17.0 | 14.0 | 17.0 | 15.0 | 18.0 | 14.0 | 17.0 | 15.0 | 16.0 | 12.0 |

| RUN | SIDE | X POSITION ON THE WATER POND | | | | | | | | | | | | | | | | | | | | | | | | | |
|---|---|---|---|---|---|---|---|---|---|---|---|---|---|---|---|---|---|---|---|---|---|---|---|---|---|---|---|
| | | 2.5 | 5.2 | 10.2 | 12.9 | 17.9 | 20.6 | 25.6 | 28.3 | 33.3 | 36 | 41 | 43.7 | 48.7 | 51.4 | 56.4 | 59.1 | 64.1 | 66.8 | 71.8 | 74.5 | 79.5 | 82.2 | 87.2 | 89.9 | 94.9 | 97.6 |
| 10 | Right | 19.0 | 17.0 | 19.0 | 16.0 | 19.0 | 18.0 | 18.0 | 16.0 | 19.0 | 17.0 | 19.0 | 17.0 | 17.0 | 15.0 | 18.0 | 16.0 | 19.0 | 17.0 | 19.0 | 17.0 | 19.0 | 17.0 | 19.0 | 17.0 | 18.0 | 16.0 |
| | Left | 20.0 | 16.0 | 15.0 | 13.0 | 16.0 | 13.0 | 18.0 | 13.0 | 18.0 | 14.0 | 21.0 | 14.0 | 19.0 | 13.0 | 16.0 | 12.0 | 19.0 | 17.0 | 19.0 | 16.0 | 20.0 | 15.0 | 20.0 | 18.0 | 18.0 | 17.0 |
| 11 | Right | 19.0 | 17.0 | 19.0 | 17.0 | 18.0 | 17.0 | 17.0 | 16.0 | 16.0 | 14.0 | 17.0 | 14.0 | 18.0 | 16.0 | 19.0 | 17.0 | 19.0 | 18.0 | 19.0 | 17.0 | 19.0 | 17.0 | 19.0 | 18.0 | 17.0 | 15.0 |
| | Left | 19.0 | 15.0 | 18.0 | 15.0 | 16.0 | 13.0 | 19.0 | 12.0 | 19.0 | 14.0 | 20.0 | 15.0 | 20.0 | 15.0 | 19.0 | 16.0 | 18.0 | 16.0 | 18.0 | 15.0 | 16.0 | 13.0 | 16.0 | 13.0 | 18.0 | 15.0 |
| 12 | Right | 17.0 | 15.0 | 19.0 | 17.0 | 19.0 | 16.0 | 17.0 | 16.0 | 17.0 | 15.0 | 17.0 | 15.0 | 19.0 | 16.0 | 17.0 | 15.0 | 19.0 | 18.0 | 18.0 | 16.0 | 17.0 | 14.0 | 18.0 | 17.0 | 18.0 | 16.0 |
| | Left | 17.0 | 14.0 | 20.0 | 15.0 | 16.0 | 14.0 | 19.0 | 14.0 | 18.0 | 14.0 | 19.0 | 14.0 | 19.0 | 15.0 | 16.0 | 13.0 | 17.0 | 13.0 | 18.0 | 16.0 | 19.0 | 15.0 | 18.0 | 15.0 | 18.0 | 15.0 |
| 13 | Right | 9.0 | 7.0 | 10.0 | 8.0 | 9.0 | 7.0 | 9.0 | 7.0 | 9.0 | 7.0 | 9.0 | 6.0 | 10.0 | 8.0 | 9.0 | 7.0 | 9.0 | 6.0 | 9.0 | 7.0 | 9.0 | 7.0 | 9.0 | 8.0 | 9.0 | 7.0 |
| | Left | 10.0 | 6.0 | 9.0 | 5.0 | 10.0 | 5.0 | 11.0 | 6.0 | 10.0 | 6.0 | 9.0 | 4.0 | 10.0 | 4.0 | 10.0 | 5.0 | 10.0 | 7.0 | 10.0 | 7.0 | 11.0 | 6.0 | 9.0 | 4.0 | 10.0 | 6.0 |
| 14 | Right | 9.0 | 7.0 | 9.0 | 7.0 | 9.0 | 7.0 | 9.0 | 7.0 | 9.0 | 6.0 | 10.0 | 7.0 | 9.0 | 6.0 | 9.0 | 7.0 | 8.0 | 7.0 | 9.0 | 7.0 | 8.0 | 6.0 | 9.0 | 7.0 | 9.0 | 7.0 |
| | Left | 10.0 | 7.0 | 11.0 | 4.0 | 10.0 | 6.0 | 11.0 | 6.0 | 10.0 | 6.0 | 9.0 | 5.0 | 9.0 | 5.0 | 9.0 | 6.0 | 9.0 | 7.0 | 9.0 | 7.0 | 9.0 | 5.0 | 10.0 | 6.0 | 10.0 | 7.0 |
| 15 | Right | 9.0 | 6.0 | 9.0 | 6.0 | 10.0 | 7.0 | 10.0 | 7.0 | 10.0 | 6.0 | 9.0 | 6.0 | 9.0 | 7.0 | 9.0 | 6.0 | 10.0 | 7.0 | 11.0 | 8.0 | 10.0 | 7.0 | 10.0 | 8.0 | 10.0 | 8.0 |
| | Left | 11.0 | 8.0 | 9.0 | 6.0 | 10.0 | 5.0 | 11.0 | 5.0 | 9.0 | 5.0 | 10.0 | 5.0 | 9.0 | 6.0 | 9.0 | 5.0 | 10.0 | 6.0 | 10.0 | 6.0 | 10.0 | 5.0 | 10.0 | 6.0 | 10.0 | 9.0 |
| 16 | Right | 10.0 | 9.0 | 10.0 | 7.0 | 9.0 | 7.0 | 10.0 | 7.0 | 10.0 | 7.0 | 10.0 | 7.0 | 9.0 | 7.0 | 11.0 | 7.0 | 10.0 | 7.0 | 10.0 | 7.0 | 10.0 | 8.0 | 10.0 | 9.0 | 9.0 | 8.0 |
| | Left | 10.0 | 7.0 | 9.0 | 5.0 | 10.0 | 8.0 | 11.0 | 6.0 | 10.0 | 5.0 | 9.0 | 6.0 | 10.0 | 5.0 | 10.0 | 5.0 | 9.0 | 5.0 | 10.0 | 7.0 | 10.0 | 5.0 | 10.0 | 6.0 | 9.0 | 7.0 |
| 17 | Right | 17.0 | 15.0 | 16.0 | 14.0 | 17.0 | 14.0 | 18.0 | 14.0 | 18.0 | 13.0 | 18.0 | 15.0 | 18.0 | 14.0 | 16.0 | 14.0 | 17.0 | 15.0 | 17.0 | 15.0 | 19.0 | 15.0 | 18.0 | 16.0 | 17.0 | 15.0 |
| | Left | 19.0 | 15.0 | 17.0 | 16.0 | 17.0 | 14.0 | 16.0 | 10.0 | 16.0 | 14.0 | 18.0 | 15.0 | 17.0 | 14.0 | 17.0 | 13.0 | 17.0 | 15.0 | 17.0 | 15.0 | 17.0 | 13.0 | 15.0 | 12.0 | 16.0 | 14.0 |

## 4.7. Time-slice for Analysis

Taking into account the short water pond length with respect to aircraft speed of the testing, the right selection of the time interval to be used is crucial to obtain reliable results.

The time intervals considered in this study were:

- **Pond in/out intervals:** defined by the video signal (24Hz) and reference visual marks on the runway that indicated when the complete MLG was inside the pond. Time marks were additionally verified with the X runway acceleration signal.

- **Brake application**: defined by brake pressure rise and drop.

- **Stabilized interval**: On un-braked tests, this interval comprises the period between pond entry and exit, discarding initial and final spurious transients on filtered signals. On the braked cases, the interval is limited to the time slice in which braking is stable (identifiable by uniform braking pressures).

Due to the initial transient on the active braking, some wheels entered the pond already braked. This triggered a second transient. Therefore, the wheels that were braked in advance of water pond entry that exhibited a strong transient were not considered valid for the analysis.

Table 10 shows the time intervals defined on the test runs.

As can be seen in the table, the typical chosen stabilized time slices are very short and far shorter than the standard braked stabilisation times required for braking performance measurement. The time slices were on the order of 0.5s. This was mainly due to the short length of the available water pond.

In addition, it was also not possible to guarantee that, in such small time intervals, it would be possible to capture completely the anti-skid stability and the braking friction that may be generated on the contaminated runway.

In spite of the short time intervals, a large volume of data was gathered, and deemed as sufficient to attempt an analysis. The time histories of forces and brake pressure show a smooth behaviour of these variables. As a result, an analysis based on these data has been carried out.




Future Sky Safety has received funding from the EU's Horizon 2020 Research and Innovation Programme, under Grant Agreement No. 640597.

| Test | Water pond interval* [s] | | Brake time* [s] | | Stabilized time* [s] | | Δ Stabilized time [s] |
|---|---|---|---|---|---|---|---|
| Run | IN | OUT | IN | OUT | IN | OUT | |
| 1 | 0.000 | 2.810 | - | - | 0.079 | 2.704 | 2.625 |
| 2 | 0.000 | 2.938 | 0.447 | 1.572 | 0.978 | 1.416 | 0.438 |
| 3 | 0.000 | 2.400 | - | - | 0.100 | 0.750 | 0.65 |
| 4 | 0.000 | 2.320 | 0.509 | 1.853 | 0.634 | 1.728 | 1.094 |
| 5 | 0.000 | 2.040 | - | - | 0.189 | 1.970 | 1.781 |
| 6 | 0.000 | 2.080 | 0.299 | 1.393 | 0.611 | 1.299 | 0.688 |
| 7 | 0.000 | 1.840 | - | - | 0.625 | 1.719 | 1.094 |
| 8 | 0.000 | 1.920 | 0.113 | 1.097 | 0.659 | 0.988 | 0.329 |
| 9 | 0.000 | 1.680 | - | - | 1.000 | 1.571 | 0.571 |
| 10 | 0.000 | 1.640 | 0.551 | 1.676 | 1.207 | 1.645 | 0.438 |
| 11 | 0.000 | 3.200 | - | - | 0.040 | 3.240 | 3.2 |
| 12 | 0.000 | 3.040 | 0.376 | 1.643 | 0.736 | 1.596 | 0.86 |
| 13 | 0.000 | 2.040 | - | - | 1.146 | 1.974 | 0.828 |
| 14 | 0.000 | 2.000 | 0.398 | 1.461 | 0.601 | 1.273 | 0.672 |
| 15 | 0.000 | 2.440 | - | - | 0.126 | 2.361 | 2.235 |
| 16 | 0.000 | 2.520 | 0.154 | 1.154 | 0.529 | 1.076 | 0.547 |
| 17 | 0.000 | 2.760 | -0.046 | 1.595 | 0.267 | 1.392 | 1.125 |

**Table 10 Time intervals defined on the test runs**

*** Origin of times (time = 0 s) is taken at the instant corresponding to pond entry.**




Future Sky Safety has received funding from the EU's Horizon 2020 Research and Innovation Programme, under Grant Agreement No. 640597.

## 4.8. Aircraft trajectory and water depth encountered

Aircraft longitudinal (X) position (as a function of time) has been obtained from the integration of ground speed data.

Lateral deviation with respect to runway centreline (Y position) was obtained from DGPS data. Local offsets were removed with the help of video recordings from a camera located in the NLG, as well as visual reference marks painted on the runway.


**Figure 44 Runway marks employed to signalize entry to the eater pond**

Water depth encountered by the front row of tires was obtained through linear interpolation on the depth data pool, by means of the methodology described in section 4.2.1.

Once aircraft trajectory and water depth were computed, the dataset was reduced to the time interval in which it was considered that all the aircraft parameters (thrust, loads, brake pressure, control surfaces) were stable (see Table 9 for more details on selected intervals).

Figure 45 shows the average depth of the four MLG front tires, according to each wheel track and the selected time slice to be analysed.




Future Sky Safety has received funding from the EU's Horizon 2020 Research and Innovation Programme, under Grant Agreement No. 640597.

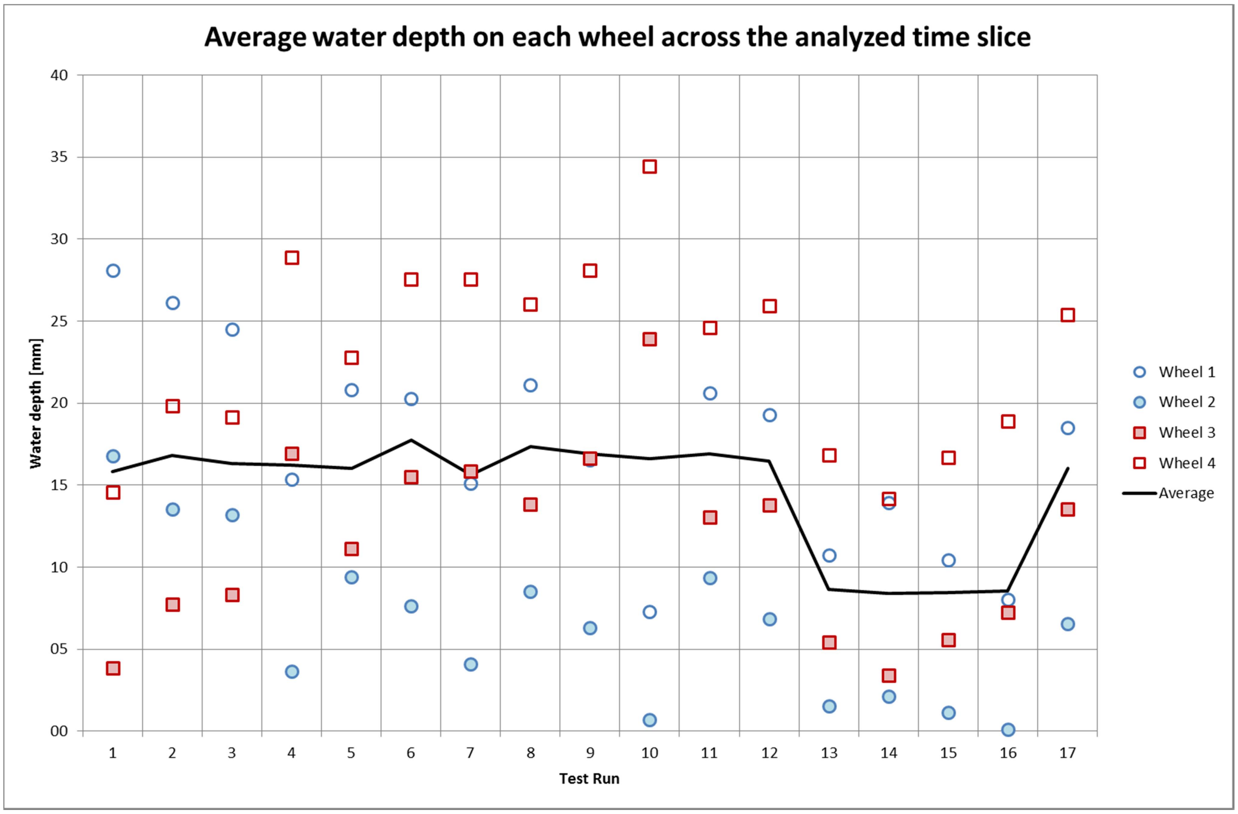


**Figure 45 Average depth of MLG front tires**

If average data are considered for the four front MLG tires, results show that tests with a target depth of 15 mm were subjected to 16.5 mm on average. Analogously, for when the target depth was 8 mm, calculated actual average depth was 8.5 mm.

At some runs, certain wheels encountered depth values lower than 6.5 mm. In these cases, due to the transversal slope and the aircraft lateral deviation, dry and wet areas were encountered along the aircraft trajectory inside the water pond. These cases were discarded for the analysis, since they were not considered representative of contaminated conditions.




Future Sky Safety has received funding from the EU's Horizon 2020 Research and Innovation Programme, under Grant Agreement No. 640597.

## 4.9. LG loads

Braking performance calculations at tire level were based on brake torque pin measurements, as well as on the estimation of horizontal and vertical forces over the wheels at aircraft axes. The latter are the result of the combination of measurements of five strain gauges at each side of the MLG.

Several issues, inherent to the use of such sensors, should be borne in mind when evaluating data quality:

- The calibration and combination of the five strain gauges is fitted for braking in standard conditions, not for conditions with high volumes of water in front of the tires. The contact point between tire and runway is different on contaminated conditions. This could impact the accuracy of the measurements, inducing error and biased results.
- After each test, the baseline static condition on each gauge changed, making it necessary to re-datum the signals. This process is complex and could introduce some further error and/or bias in the results.
- Some of the measurements aim to estimate forces that are equal or below the measurement threshold. When the tire rolls on un-braked conditions at low speeds, or brakes above aquaplaning speed, the horizontal loads could be below the working range of the sensors.
- The measurements rely strongly on shock absorber stroke values. The shock conditions on the aircraft, as well as **aircraft lateral imbalance** due to the heavy FTI installed, could lead to error and/or bias between left and right sides of the MLG.

Therefore, in some areas, the results maybe just indicative, and the validity of the analysis shall come not only from the measurements but also from the qualitative comparison with other analysis methods and from previous flight test data on other platforms (i.e. NLR Cessna Citation previous contaminated test in Twente Airport).




Future Sky Safety has received funding from the EU's Horizon 2020 Research and Innovation Programme, under Grant Agreement No. 640597.

## 4.10. Test analysis

### 4.10.1 Introduction

This section presents the results of the analysis of the deceleration forces present on water contaminated runways. The different sub-chapters specify the results gathered to build models for:

- Displacement drag
- Braking friction
- Aquaplaning speed
- Displacement drag under aquaplaning conditions

Data was processed individually for each wheel in the MLG front axle. Only the wheels considered to be rolling on contaminated conditions (average water depth > 6.5 mm, with no large wet or dry zones) were taken into account for the assessment of displacement drag and braking friction. Similarly, only those wheels not affected by aquaplaning were taken into account for the calculation of braking friction and displacement drag. The status of each wheel is specified in Table 5.

The analysis presented here is based on the calculated depths encountered by the tires, aircraft ground speed and MLG loads (horizontal, vertical and braking torque), as well as the tire deflections. This information was also used to estimate the exposed surface of the tire in contact with the water, the point of application of the braking force and the slip ratio of the tires.

The data processed in this study was analyzed on the available time intervals (see Table 9) and averaged over time.

As previously commented on Section 4.5, the conditions in which the strain gauges were used reduced their accuracy. As a result, an increased scatter and bias is expected to be found. To minimize the potential impact of this issue, comparisons with previous NLR tests, performed on the same runway were conducted, showing consistent results. In addition, results were compared with ESDU 90035 models for displacement drag on a single tire, in order to provide a context for their evaluation.

### 4.10.2 Displacement Drag Model

The next Figure 46 shows the displacement drag calculated for front wheels (1 to 4) with red circles.

Represented data has been obtained from the eight un-braked test results, taking into account only those tires that met two conditions:

- Contaminated conditions (depth > 3 mm) were present along the complete path inside the pond.
- Aquaplaning was not registered.

The first condition was assessed by checking depth distributions for each wheel, and discarding those which encountered large dry or wet sections, or subjected to an average depth lower than the minimum target depth value (8 mm). In order to allow for larger data availability, all tests with an average depth equal or beyond 6.5 mm which showed no (or insignificant) dry/wet zones were considered valid.

Regarding the second condition, it was considered that aquaplaning condition was met when tire slip ratio reached values below 0.5, in absence of braking pressure. As a result of these two constraints, 16 wheel performance test cases (from a total of 32 [t wheels x 8 un-braked runs]) were considered valid for the analysis.

Displacement drag of valid wheels was calculated as follows.

- First of all, X load measurements for each MLG leg (once properly filtered) were projected in runway X axis.
- Then, rolling friction ($\mu_{Roll}$) contribution to horizontal retarding force was estimated. In order to do this, it was necessary to assess rolling friction force on dry conditions. This is possible, due to the availability of aircraft data before pond entry. In order to avoid undesirable noise and scatter in the evaluation of $\mu_{Roll}$, only sections with stabilized thrust and acceleration were considered for the analysis.
- Finally, calculated rolling friction was subtracted from projected X loads, yielding an estimation of displacement drag for each wheel.

As previously stated, displacement drag has been represented as a function of average depth and average GS of the run (Figure 46). Based on this data, a two dimensional, third order regression was built to estimate displacement drag as a function of these two variables. This model is represented by the blue/yellow grid in Figure 46.




Future Sky Safety has received funding from the EU's Horizon 2020 Research and Innovation Programme, under Grant Agreement No. 640597.

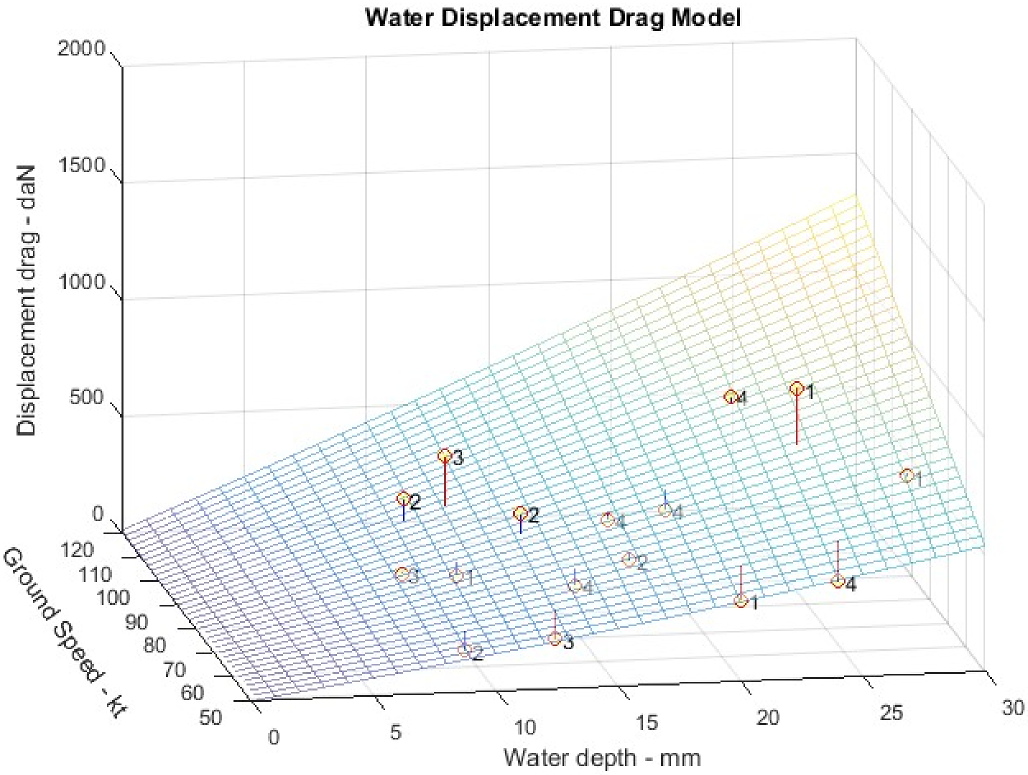


**Figure 46 Displacement drag of front axle wheels, and regression model based on these measurements**

Due to the amount of data gathered, it was not possible to include the impact of the tire deflection. Nevertheless, it can be observed that calculated displacement drag fits the model relatively well (within sensors accuracy), as proven by the red lines that show discrepancy between model and calculations.

Finally, a comparison has been established between this regression and ESDU 90035 model for displacement drag on a single tire (Ref. [2]). This model estimates displacement drag as a function of contaminant depth, GS and tire deflection. The difference in estimated displacement drag between models (ESDU and regression) is plotted in Figure 47. This plot shows the displacement drag predicted by the previously presented regression model minus that predicted by ESDU 90035. It can be concluded that obtained displacement drag fits both models with the same accuracy level (regression and ESDU 90035). Nevertheless, the regression model predicts a higher displacement drag at low speeds and high depths, which allows for a higher conservatism.




Future Sky Safety has received funding from the EU's Horizon 2020 Research and Innovation Programme, under Grant Agreement No. 640597.

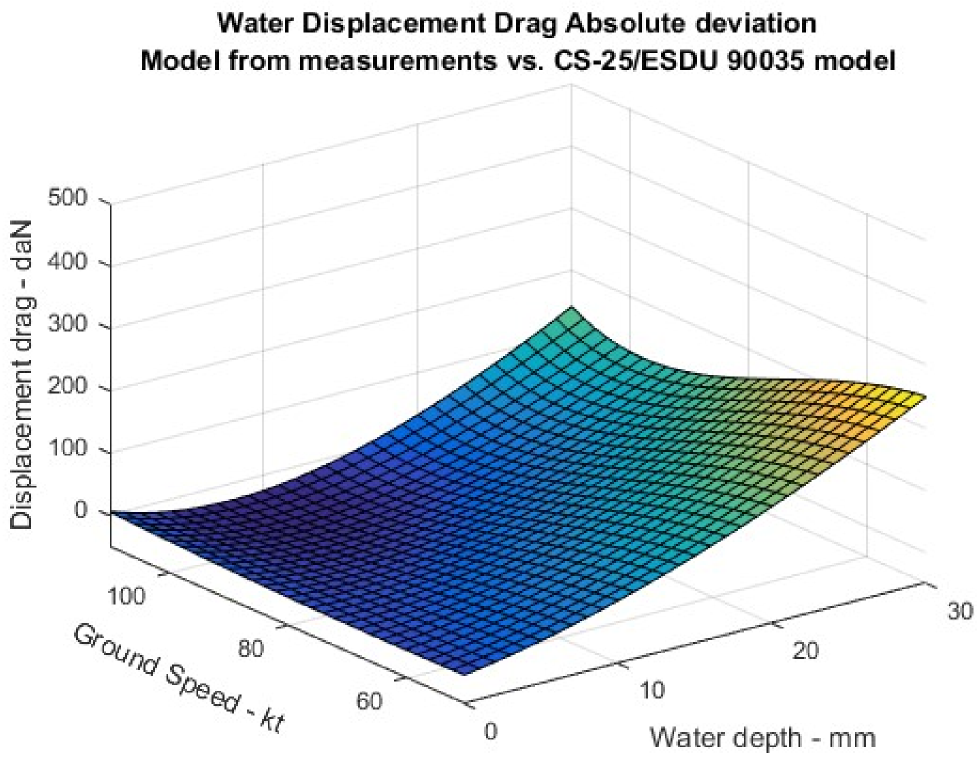


**Figure 47 Difference of estimated displacement drag between models (ESDU 90035 and regression)**

### 4.10.3 Aquaplaning speed

When a single tire rolls over a water-covered surface of sufficient depth, two hydrodynamic forces are generated on the tire tread:

- Hydrodynamic "drag" (commonly known as "displacement drag"), parallel to the surface of the tire tread. This is further discussed in the present document as one of the main sources of retarding horizontal force in contaminated operations, and can be modelled as:

$$D_h = \frac{1}{2}\rho_w V^2 S_{ref\,D} C_{Dh} \quad \text{(Eq. 4)}$$

- Hydrodynamic "lift", normal to the surface of the tire tread, which can be modelled as:

$$L_h = \frac{1}{2}\rho_w V^2 S_{ref\,L} C_{Lh} \quad \text{(Eq. 5)}$$

It is precisely this second component the one with relevance for the development of aquaplaning.

Taking into account that water is an incompressible fluid, and assuming that the changes in hydrodynamic lift coefficient $C_{Lh}$ and contact surface $S_{refL}$ will be small enough to regard them as constant, variations in hydrodynamic lift will be mainly dependent on speed.

Dynamic aquaplaning takes place when "lift" force generated by the contaminant layer equals total download on the wheel. In other words, when the equivalent pressure generated by hydrodynamic lift over the contact surface equals the tire bearing pressure (Ref. [3]). This is expressed below:

$$\frac{L_h|_{V_p}}{S}=\frac{1}{2}\rho_w V_p^2 C_{Lh}=p_{\text{bearing tire}} \quad \text{(Eq. 6)}$$

The tire loses contact with the ground, and is entirely sustained by the fluid layer. As expressed in equation 6, the value of ground speed at which this phenomenon is fully developed is regarded as **aquaplaning speed ($V_p$)**.

As a result of contact loss, both friction and retarding forces due to contaminant drag experiment a dramatic decrease, higher as ground speed keeps increasing beyond aquaplaning speed (Ref. [1]).

Literature and regulations (Ref. [1], Ref. [3],) characterize $V_p$ as a function only of tire inflation pressure. Recalling equation 6, aquaplaning speed can be expressed as:

$$V_p=\sqrt{\frac{2}{\rho_w C_{Lh}}}\sqrt{p_{\text{bearing tire}}}\cong K\sqrt{p_{\text{bearing tire}}} \quad \text{(Eq. 7)}$$

Where K represents a constant to be determined in terms of the type of contaminant and tires.

According to (Ref. [3]), tire bearing pressure can be accurately represented by inflation pressure, $p_{tire}$. As a result, models for aquaplaning speed are usually of the form

$$V_p=K\sqrt{p_{\text{tire}}} \quad \text{(Eq. 8)}$$

where K is the aquaplaning speed factor.

Although, for a given contaminant, hydrodynamic lift is basically a function of ground speed only, the development of aquaplaning is not solely dependent on this parameter. In fact, if water can be drained from below the tires reasonably fast, dynamic aquaplaning will not take place, or at least will not develop completely (Ref. [3]). As stated in (Ref. [3]), drainage capacity is mainly a function of tire tread characteristics and runway surface macrotexture

The estimation of $V_p$ may be one interesting output of the analysis. The detection of an exact value by means of flight testing is a highly complex task. On the one hand, it would require a very precise flight test grid which contemplated very small increments in target ground speeds of subsequent runs. On the other hand, pilot control of ground speeds would need to be excessively severe. As can be seen in the achieved test grid (table 3), differences between desired and achieved ground speeds can reach 2-3 kt. This suggests the possible impracticability to develop such a test campaign.

Nevertheless, it is possible to obtain a reasonably precise delimitation of the range of ground speeds among which aquaplaning may develop. This was the selected approach for this analysis.

One of the most evident effects of aquaplaning is **strong spin-down** of wheels. In fact, certain sources suggest a simple qualitative criterion for the detection of full dynamic aquaplaning: the identification of wheel speed values more than 50% lower to those expected in dry operations.




Future Sky Safety has received funding from the EU's Horizon 2020 Research and Innovation Programme, under Grant Agreement No. 640597.

As a result, an easy way to identify aquaplaning speed is simply the tracking of wheel speed and ground speed, and the identification of points in which a sudden decrease in the first one takes place.

A very convenient way to study the behavior of wheel speed with respect to ground speed is to define the parameter **slip ratio**:

$$\text{Slip ratio}=\frac{\text{vehicle speed-wheel speed}}{\text{vehicle speed}}=1-\frac{\omega R}{GS} \text{ (Eq. 9)}$$

In order to provide a context for this parameter, some reference values might be helpful. A slip ratio equal to zero represents a free-rolling condition, in which rotational speed equals ground speed. A slip ratio equal to 1 represents a blocked wheel, in which no rolling takes place.

At this point, it must be borne in mind that spin down is physically different in braked and un-braked operations. In braked, spin down is (at least partially) artificially induced by the application of a braking torque contrary to the sense of rotation of the wheel. Even if the wheel is not aquaplaning, a slip ratio higher than zero is expected to appear. Of course, in un-braked operations, this does not take place. Slip ratio in non-aquaplaning conditions is expected to be, if not zero, very close to it (near free-rolling conditions). This may hint the necessity of a separate analysis for braked and un-braked runs in terms of wheel speed assessment.

Aquaplaning assessment was performed, for the front axis MLG wheels (1-4), which will be subjected to substantial amounts of water.

Taking into account the wide depth variability in the present test campaign, it can be possible to encounter runs in which not all wheels experience aquaplaning simultaneously. According to depth distributions provided in section 4.2.2, outer wheels (1 and 4) are more susceptible than inner ones to encounter this condition, given the higher depths they are subjected to.

The following figures represent the evolution of slip ratio inside the pond for front axis wheels. Inner wheels (2 and 3) are represented by dashed lines, whereas outer wheels (1 and 4) are represented by solid lines. Magenta stands for left side wheels (1 and 2), whereas green stands for right side wheels (3 and 4).

Blue lines are provided as a reference of representative slip ratio values. In particular, the dashed one represents the qualitative reference for aquaplaning explained earlier in this section (rotation speed 50% lower than ground speed), which corresponds to a slip ratio=0.5.




Future Sky Safety has received funding from the EU's Horizon 2020 Research and Innovation Programme, under Grant Agreement No. 640597.

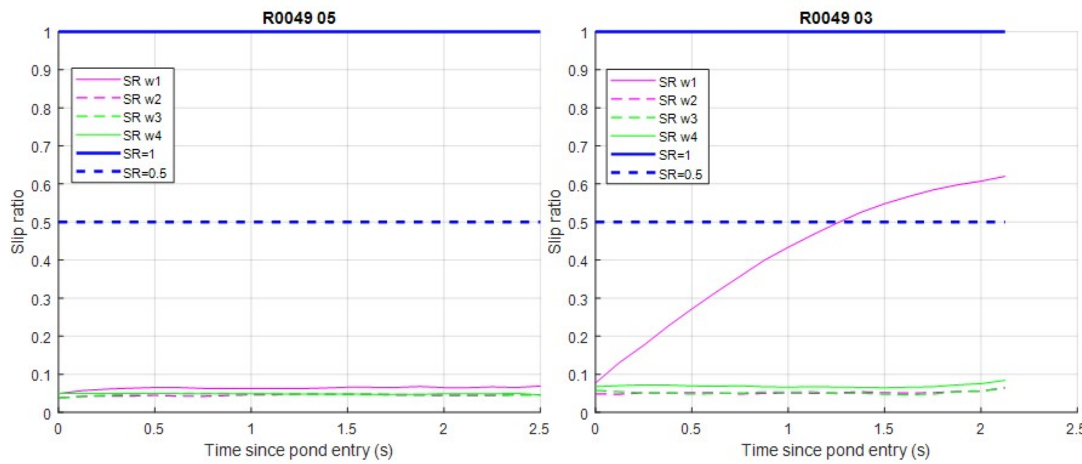


**Figure 48 Comparison of un-braked runs at low water depth (target depth = 8 mm) at a target GS of 80 kt (left) and 90 kt (right)**

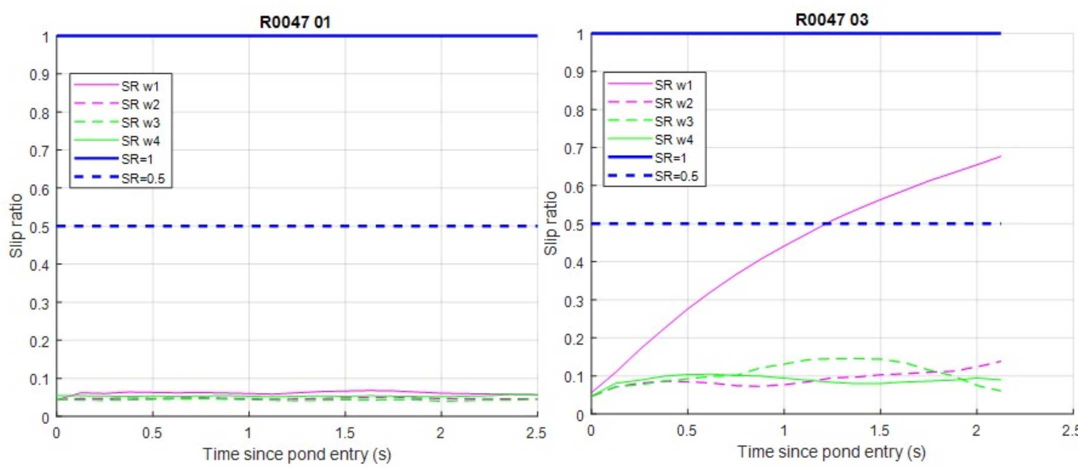


**Figure 49 Comparison of un-braked runs at high water depth (target depth = 15 mm) at a target GS of 80 kt (left) and 90 kt (right)**

Figures 48 and 49 show the behavior of slip ratio in un-braked runs between 80 and 90 kt. At 80 kt, none of the wheels aquaplane, whereas at 90 kt, wheel 1 shows fully developed dynamic aquaplaning. It should be noted that this behavior is the same in with low (8 mm) and high (15 mm) depths of water. A reasonable hypothesis that could be extracted from these results is that, for each possible combination of tires and runway, there will be a “threshold” depth value above which it will not be possible to remove water quickly enough, and dynamic aquaplaning will take place from ground speeds below $V_p$. In contrast, if that “threshold” value is not exceeded, drainage may be effective enough to avoid aquaplaning, even if ground speed is higher than $V_p$. In this case, it could be suggested that, once the “drainage threshold” depth has been exceeded, a lower depth does not decrease the risk of developing aquaplaning. As a result, no relevant difference in behavior is seen between runs subjected to remarkably different contaminant depths.

As can be seen, **aquaplaning develops between 80 and 90 kt**. This is consistent with Cessna Citation test results. At 80 kt, none of the wheels aquaplane, whereas at 90 kt, wheel 1 always shows fully developed dynamic aquaplaning.

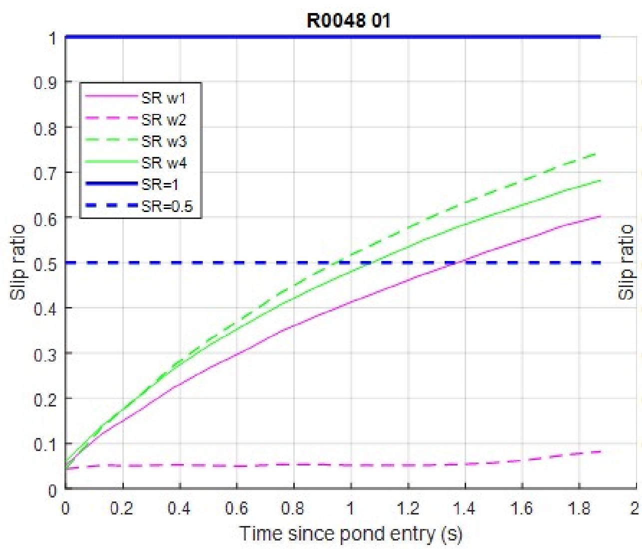


**Figure 50 Un-braked run at a target GS of 100 kt at high water depth (target depth = 15mm**

As ground speed continues increasing beyond aquaplaning speed, wheels 3 and 4 also show full dynamic aquaplaning. This can be seen in previous Figure 50. The fact that right side wheels need a higher ground speed to develop aquaplaning may be justified due to the lateral imbalance presented by the test aircraft due to FTI. In any case, this could be an indication that the normal load on these tires is higher, and this displaces the development of full dynamic aquaplaning to higher speeds. This may also suggest that, in some cases, inflation pressure may not provide an accurate estimate of the normal load tires are subjected to.

Figure 51 shows the behavior for the highest GS tested in the campaign (target 110 kt).




Future Sky Safety has received funding from the EU's Horizon 2020 Research and Innovation Programme, under Grant Agreement No. 640597.

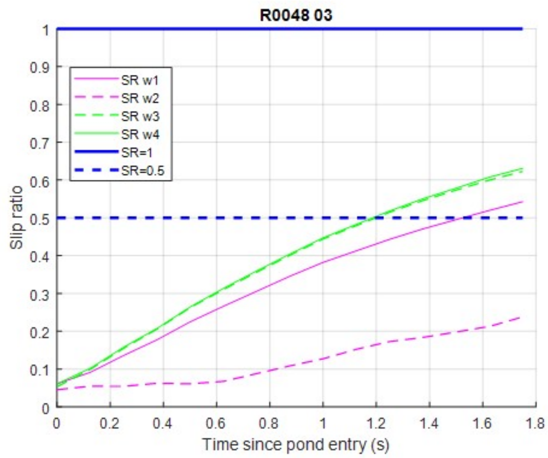


**Figure 51 Un-braked run at a target GS of 110 kt at high water depth (target depth = 15mm)**

Furthermore, although wheels 1, 3, and 4 show full dynamic aquaplaning beyond 100 kt, wheel 2 does not show aquaplaning; at the most, a slight spin down (slip ratio increase). This may be justified by the considerably lower water depth (in both average and local terms) this tire is subjected to. As mentioned previously in this section, in order for dynamic aquaplaning to develop, two conditions must be met:

1. GS must be high enough so that aquaplaning lift force is able to counteract total download on the wheel.
2. Contaminant depth must be high enough so that the combined effect of tire tread and runway surface macrotexture is insufficient for drainage.

As a result, if the tread is able to drain the water underneath, no aquaplaning will take place, no matter how high the ground speed is. Wheel 2 is subjected to low depths, including wet (<3 mm water) and even dry zones. As a result, it is not representative for aquaplaning speed determination.

Evidence of this statement is provided in Figure 52. It provides a very simple, schematic representation, on contaminated (depth > 3 mm), wet (depth < 3 mm) and dry areas each of the front wheels is subjected to in run R048_04 (target GS =110 kt). As can be seen, wheel 2 is subjected to large wet and dry areas, whereas the remaining wheels see little or no non-contaminated zones.




Future Sky Safety has received funding from the EU's Horizon 2020 Research and Innovation Programme, under Grant Agreement No. 640597.

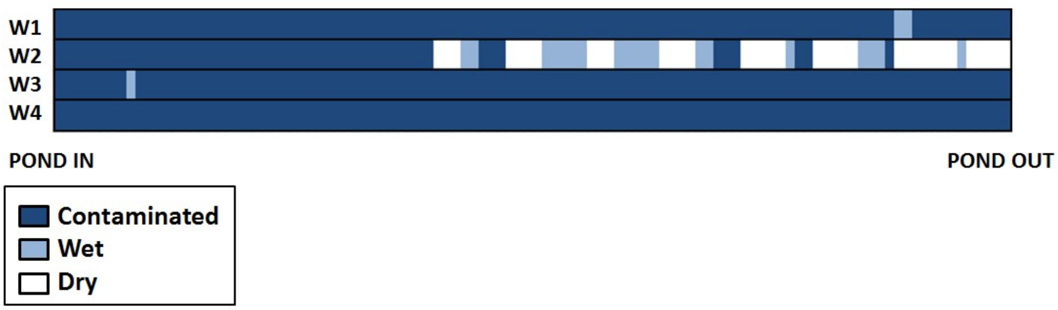


**Figure 52 Schematic representation of dry, wet and contaminated zones for the four front wheels of run R0048_04.**

At low speeds, dynamic aquaplaning is unlikely to occur, but viscous aquaplaning could take place if the runway is not well maintained or its microtexture is insufficient (Ref. [3]). Figure 53, corresponding to a target GS of 70 kt, show no signs of aquaplaning. This could be taken as a proof of the lack of viscous aquaplaning, and, in consequence, as evidence of the runway being properly maintained and having sufficient microtexture.

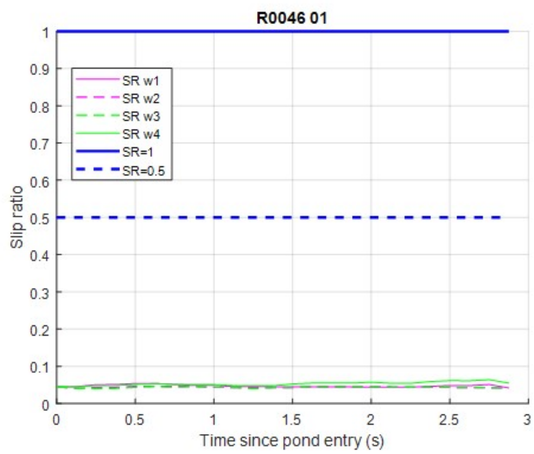


**Figure 53 Un-braked run at a target GS of 70 kt at high water depth (target depth = 15mm)**




Future Sky Safety has received funding from the EU's Horizon 2020 Research and Innovation Programme, under Grant Agreement No. 640597.

### 4.10.4 Contaminant drag above aquaplaning speed

Once the speed surpasses $V_p$, displacement drag diminishes proportionally to the ratio $GS/V_p$ (Ref. [1])

Under these circumstances, the wheels roll over the water. The amount of displaced water decreases, and the angle of water projection changes from forward (the so called bow wave) to backward. The following Figures 54, 55 and 56 show this evolution, with the aircraft rolling around 80 kt (before aquaplaning), 90 kt (very close to aquaplaning transition speed), and 110 kt (front row fully aquaplaning).

**Figure 54 Aircraft rolling at 80kt. Bow wave is clearly visible.**


**Figure 55 Aircraft rolling at 90kt. Front tires transition to aquaplaning**




Future Sky Safety has received funding from the EU's Horizon 2020 Research and Innovation Programme, under Grant Agreement No. 640597.


**Figure 56 Aircraft rolling at 110kt. Water is projected backwards.**

The data analyzed was coherent with this observation. Figure 57 shows the average displacement drag measured in un-braked tests around 100kt and 110kt. Only test cases in which both sides of the MLG were aquaplaning were taken into consideration. This way, the potential impact of aircraft lateral imbalance is minimized. As in the displacement drag analysis, the data comes from the MLG X loads. This parameter was subjected to the aforementioned uncertainties at the time of determining the offsets (as described in section 4.5).

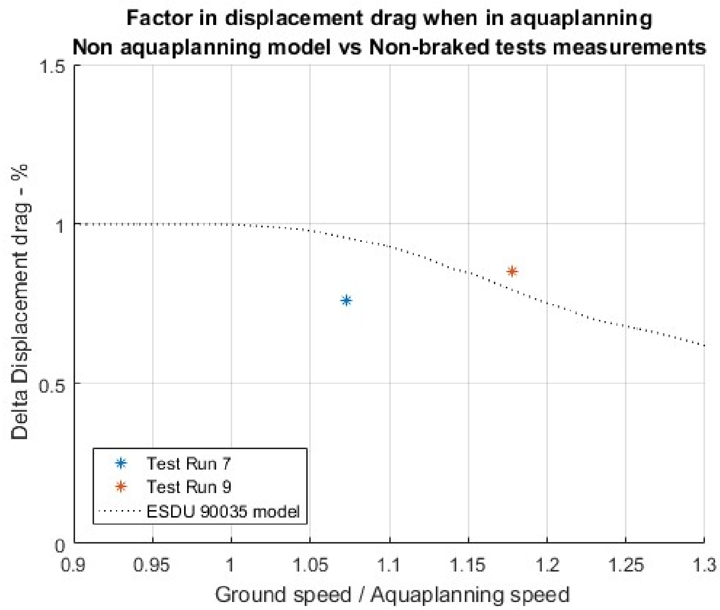


**Figure 57 Displacement drag factor as a function of GS/Vp**

The figure represents the factor measured (Displacement Drag / Displacement Drag at $V_p$) versus the factor (GS/reference $V_p$). Reference $V_p$ has been considered equal to $8\sqrt{p_{tire}}$, where $p_{tire}$ represents the average tire inflation pressure along the tests (141 psi). This $V_p$ model has been taken from (Ref. [3]), as representative for modern bias ply tires. Colored points show test results, whereas the dotted line represents the model from ESDU 90035, Ref. [2]. If the factor 8 was reduced to a value closer to what was observed in the tests ($V_p$ between 80 and 90 kt, which would yield a factor between 6.7 and 7.6 for the aforementioned tire pressure), the points would present a better fitting with the ESDU model, and both test runs would show the same distance to it. In any case, the displacement drag at test run 9 (112 kt) is very high, and no other reason apart from the accuracy of the X load accuracy was found to explain this behavior.

### 4.10.5 Braking friction model

Figure 58 below shows the effective braking friction measured on wheels 1 to 4 (front tires) in blue circles. This data comes from the braked tests, on the tires that rolled consistently on contaminated conditions, independently of whether aquaplaning was present or not.

As in the previous displacement drag analysis, non-contaminated conditions were considered for all the tires that rolled on an average water depth not higher than 6.5mm.

The direct brake torque pin method was chosen for the analysis. It is known that the use of torque measurements introduces uncertainties due to the unknown tire deflected radius. Nevertheless, this procedure presents an interesting advantage: it allows for a much more direct measurement of braking friction, in contrast with the X loads method, which requires an accurate displacement drag model to be subtracted from the measurements.

The theoretical approach when using the brake torque pin measurement is the use of moment equilibrium at tire level, considering the following assumptions:

- a negligible change in the position of the contact pressure center, $x_c$, when changing from non-braked to braked conditions. This is reasonable, taking into account the expected low braking capability (not possible to ensure without further testing).
- a negligible value of $I\frac{d\omega}{dt}$, considering the low change in speed in the short braking period (as proved in the tests).
- almost constant slip ratio values (as proved in the tests).

In this case, the moments balance on the rolling case would be:

$$I\frac{d\omega}{dt}=\left(X_{Rolling}+X_{Contaminant}\right)r_d-Z\cdot x_c\approx 0 \quad \text{(Eq. 10)}$$

And the moments balance on the braked case would be:

$$I\frac{d\omega}{dt}=\left(X_{Rolling}+X_{Braking}+X_{Contaminant}\right)r_d-Z\cdot x_c-M_{Brake}\approx 0 \quad \text{(Eq. 11)}$$

Resolving the first equation into the second, it yields:

$$\eta_{A/S}\cdot\mu_{Brake}=\frac{M_{Brake}}{Z\cdot r_d} \quad \text{(Eq. 12)}$$

Nevertheless, it was considered that, due to friction being an effect of both rolling (wheel deformation) and braking (braking torque application), the effective braking coefficient $\mu_{eff}$ should take into account both effects:

$$\mu_{effective}=\frac{M_{Brake}}{Z\cdot r_d}+\mu_{Roll} \quad \text{(Eq. 13)}$$

The value of $\mu_{Roll}$ used was estimated from dry rolling data, by means of the method described in section 4.2.1.

Once the effective braking friction on each wheel had been determined, it was necessary to consider the architecture of the MLG braking system. In this case, brake pressure is not individually controlled in each wheel, but in common for each pair of wheels on each axle. Three different scenarios can be considered. Depending on the one which was applicable for each case, only one braking friction value was retained for each pair of wheels:

- **Case 1:** both tires roll on contaminated runway conditions. The braking pressure is limited by the tire that encounters the maximum friction earlier. Therefore, the maximum braking friction measured on each pair of wheels is retained. Normally, as seen in flight tests, the limitation arises in the inner wheels.

- **Case 2:** both tires are in contaminated runway conditions, one rolling properly and the other aquaplaning: The wheel that is not aquaplaning does not brake either, since the strong skidding in the wheel subjected to aquaplaning makes the anti-skid system release almost completely the braking pressure. The data on the wheel which was not aquaplaning was discarded for the braking coefficient analysis.

- **Case 3:** one tire rolls on contaminated conditions and the other on wet ones. The wheel under contaminated conditions reached the friction limitation before the one in wet conditions. The data on the wet wheel was discarded, only the data on the wheel on contaminated conditions was used.

Additionally, to minimize the potential impact of inaccurate biases in vertical loads between left and right MLG sides, the results from both sides was averaged and only a single point per test was shown. Some information is lost on this averaging: the test with only one side braking in the considered appropriate conditions. Additionally, also the information of the water depths is lost. Along the testing, due to the runway transversal slope and the aircraft lateral deviation, very different water depths were found on the points limiting the friction. The results presented in figure 58 show that no observable relationship between braking friction and water depth was evident.

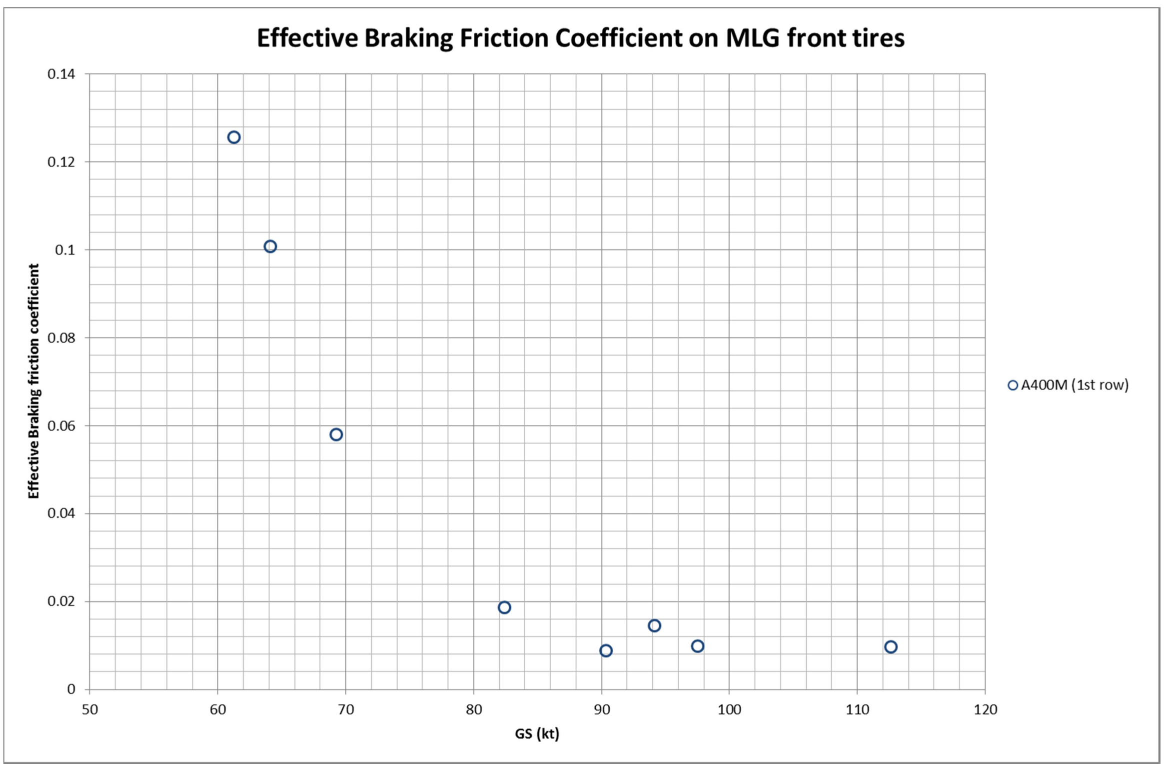


**Figure 58 Effective Braking Friction Coefficient as a function of GS, calculated for A400M MLG front tires**




Future Sky Safety has received funding from the EU's Horizon 2020 Research and Innovation Programme, under Grant Agreement No. 640597.

# 5 CONCLUSIONS

## 5.1. Flight test results obtained with a Business Jet

A substantial number of tests with specially instrumented Cessna Citation II aircraft have been conducted on a flooded runway condition. These tests were conducted as part of Project P3 of the Future Sky Safety Programme to obtain flight test data and a better understanding of aircraft ground handling performance flooded runway conditions.

Major test findings are:

- Ground speed was identified as major a factor that influences flooded-runway tyre friction performance;
- The tyre friction performance for flooded runway conditions is significantly less than for a wet runway;
- Braking capabilities for a water depth of 9.9 mm is comparable to that for 16.7 mm depth.
- Hydroplaning has a large influence on the anti-skid performance of the Cessna Citation test aircraft. It is shown that locked wheel conditions can occur despite the locked wheel crossover protection system.

## 5.2. Flight test results obtained with a Large Transport Aircraft

The flight test campaign consisted of 17 test points (8 braked, 8 non-braked and the repetition of one of the braked runs).

All of them were considered valid for the analysis of braking performance at tire level.

Several sources of error have been highlighted throughout the document.

- Water depth non-homogeneity required the definition of a precise procedure for depth calculations, as well as a careful assessment of individual wheel tracks.
- The limited pond length (100 m) leaded to short data recording intervals
- The calibration of landing gear loads increased data error, and may have introduced bias in the results.

Nevertheless, the high sampling-rate of the parameters of interest allowed for a considerable amount of data to be gathered.

In addition to this, results show consistency with previous tests performed by NLR on the same runway.

Regarding test findings, four main points are to be highlighted:

- In terms of **displacement drag**, a 3$^{rd}$ order regression was built, as a function of both ground speed and average depth seen by the wheel. This shows adequate consistency with the model proposed by ESDU 90035 (Ref. [2]).




Future Sky Safety has received funding from the EU's Horizon 2020 Research and Innovation Programme, under Grant Agreement No. 640597.

- In terms of **aquaplaning speed**, if the most conservative results are considered, aquaplaning is estimated to take place between 80 and 90 kt. This is consistent with the results obtained by NLR in their Cessna Citation tests (which estimated aquaplaning to occur between 84 and 92 kt.
- In terms of **rolling friction**, its measurements during the test campaign were consistent with the expected results. In consequence, they were used for the estimation of effective braking friction coefficient.
- In terms of **braking friction**, results at tire level indicated, as in the case of aquaplaning speed, consistency with previous tests performed on the same runway.

## Acknowledgements

*Flight testing cannot be done by just a few people. It involves the cooperation of many persons, each having an essential task. In case of the water pond flight tests described in this report, more than 40 persons were involved during each of the flight tests. These include the test pilots (from NLR and Airbus), the flight test engineers (from NLR and Airbus), the ground mechanics (from NLR and Airbus), the staff that supported the operation of the water pond, the fire brigade, the airport supporting staff, staff from the water supplier, and the hangar crew from NLR and Airbus that prepared the test aircraft. The authors would like to thank all these persons for their hard work. Without their support the flight tests simply could not have been conducted.*

# 6 REFERENCES

1. Certification Specifications (CS) 25 – Acceptable Means of Compliance (AMC) 25.1591 Amendment 2;
2. ESDU 90035: Frictional and retarding forces on aircraft tyres Part V: Estimation of Fluid Drag Forces;
3. G.W.H. van Es; Review of the state of current knowledge regarding tyre braking performance, antiskid systems, and modern aircraft tyres on water contaminated runways. Future Sky Safety D3.2, 2016.

.




Future Sky Safety has received funding from the EU's Horizon 2020 Research and Innovation Programme, under Grant Agreement No. 640597.